HHS Public Access

Author manuscript

Pharmacol Res. Author manuscript; available in PMC 2019 November 26.

Published in final edited form as:

Pharmacol Res. 2019 April ; 142: 267–282. doi:10.1016/j.phrs.2019.02.002.

Brain permeant and impermeant inhibitors of fatty-acid amide hydrolase suppress the development and maintenance of paclitaxel-induced neuropathic pain without producing tolerance or physical dependence in vivo and synergize with paclitaxel to reduce tumor cell line viability in vitro

Richard A. Slivicki[a,b], **Zhili Xu**[b], **Sonali S. Mali**[b], **Andrea G. Hohmann**[a,b,c,*]

[a]Program in Neuroscience, Indiana University, Bloomington, IN, United States

[b]Department of Psychological and Brain Sciences, Indiana University, Bloomington, IN, United States

[c]Gill Center for Biomolecular Science, Indiana University, Bloomington, IN, United States

Abstract

Activation of cannabinoid CB_1 receptors suppresses pathological pain but also produces unwanted side effects, including tolerance and physical dependence. Inhibition of fatty-acid amide hydrolase (FAAH), the major enzyme catalyzing the degradation of anandamide (AEA), an endocannabinoid, and other fatty-acid amides, suppresses pain without unwanted side effects typical of direct CB_1 agonists. However, FAAH inhibitors have failed to show efficacy in several clinical trials suggesting that the right partnership of FAAH inhibition and pathology has yet to be identified. We compared efficacy of chronic treatments with a centrally penetrant FAAH inhibitor (URB597), a peripherally restricted FAAH inhibitor (URB937) and an orthosteric pan-cannabinoid agonist (WIN55,212–2) in suppressing neuropathic pain induced by the chemotherapeutic agent paclitaxel. Each FAAH inhibitor suppressed the development of paclitaxel-induced neuropathic pain and reduced the maintenance of already established allodynia with sustained efficacy. Tolerance developed to the anti-allodynic efficacy of WIN55,212–2, but not to that of URB597 or URB937, in each dosing paradigm. Challenge with the CB_1 antagonist rimonabant precipitated CB_1-dependent withdrawal in paclitaxel-treated mice receiving WIN55,212–2 but not URB597 or URB937. When dosing with either URB597 or URB937 was restricted to the development of neuropathy, paclitaxel-induced allodynia emerged following termination of drug delivery. These observations suggest that both FAAH inhibitors were anti-allodynic rather than curative. Moreover, neither URB597 nor URB937 impeded the ability of paclitaxel to reduce breast (4T1) or ovarian (HeyA8) tumor cell line viability. In fact, URB597 and URB937 alone reduced 4T1 tumor cell line viability, albeit with low potency, and the dose matrix of each combination with paclitaxel was synergistic in reducing 4T1 and HeyA8 tumor cell line

*Corresponding author at: Department of Psychological and Brain Sciences, Indiana University, 1101 E 10th Street, Bloomington, IN 47405-7007, United States., hohmanna@indiana.edu (A.G. Hohmann).

Conflict of interest statement

The authors have no financial or otherwise conflicts of interest to declare.

viability according to Bliss, Highest Single Agent (HSA) and Loewe additivity models. Both FAAH inhibitors synergized with paclitaxel to reduce 4T1 and HeyA8 tumor cell line viability without reducing viability of non-tumor HEK293 cells. Neither FAAH inhibitor reduced viability of non-tumor HEK293 cells in either the presence or absence of paclitaxel, suggesting that nonspecific cytotoxic effects were not produced by the same treatments. Our results suggest that FAAH inhibitors reduce paclitaxel-induced allodynia without the occurrence of CB_1-dependence in vivo and may, in fact, enhance the anti-tumor actions of paclitaxel in vitro.

Keywords

Paclitaxel; Fatty-acid amide hydrolase; Cannabinoid; HeyA8; 4T1; Chemotherapy-induced neuropathic pain

1. Introduction

The endocannabinoid system, which consists of cannabinoid receptors (i.e. CB_1, CB_2) and their endogenous ligands (i.e. anandamide and 2-arachodonoylglycerol), has been the target for a number of drug discovery efforts aimed at treating chronic pain [1]. However, direct CB_1 receptor activation can result in unwanted side effects including tolerance, withdrawal and nausea [2]. Inhibitors of endocannabinoid deactivation have been developed in drug discovery efforts aimed at harnessing therapeutic efficacy of the endocannabinoid signaling system while circumventing unwanted side-effects that occur with direct CB_1 receptor activation. These compounds include inhibitors of both fatty-acid amide hydrolase (FAAH) [3], the major hydrolytic enzyme of the endocannabinoid anandamide (AEA), and monoacylglycerol lipase (MGL) [4], the primary hydrolytic enzyme responsible for the degradation of 2-arachidonylglyercol (2-AG). Both AEA and 2-AG bind to both cannabinoid receptors, whereas 2-AG binds preferentially to CB_2 relative to AEA [5]. Genetic deletion or chronic inhibition of MGL is efficacious in reducing neuropathic pain, but ultimately results in functional CB_1 receptor tolerance and dependence [6,7]. By contrast, FAAH inhibitors show efficacy in preclinical models of pain [8,9], nausea [10], and anxiety [11,12] without the occurrence of tolerance [6,13]. Whether repeated dosing with FAAH inhibitors could themselves produce signs of physical dependence in the presence of a pathological pain remains unknown. The impact of CNS-penetrant FAAH inhibitors on physical dependence, such as that induced by Δ^9-tetrahydrocannabinol, has typically been assessed in the absence of a pathological pain state [13]. Moreover, pathological pain states and chemotherapeutic treatment, themselves, can alter endocannabinoid tone [8]. For example, the platinum-derived chemotherapeutic agent cisplatin alters endocannabinoid tone in both the CNS and periphery [8]. FAAH inhibitors also have widespread physiological effects that can impact sleep [14], metabolism, among other physiological functions [15].

A recent report suggests that FAAH inhibition is efficacious in suppressing symptoms associated with cannabis use disorder [16]. However, despite demonstrated preclinical antinociceptive efficacy of FAAH inhibitors, clinical translation for pain has remained elusive. FAAH inhibitors did not exhibit significant efficacy in several phase II clinical trials of osteoarthritis [17], painful diabetic neuropathy [18], pelvic pain and bladder dysfunction

[19] despite being well tolerated with little to no adverse events reported in each of these studies. Most strikingly, the FAAH inhibitor BIA10–2474 left one dead and four others with severe neurological symptoms [20]. However, this compound binds to a number of other serine hydrolases not exhibited by other FAAH inhibitors evaluated clinically [17] and interactions with proteins other than FAAH are likely to mediate these extreme adverse events [21]. These observations highlight the need for evaluating both efficacy and possible unwanted side effects associated with chronically administered FAAH inhibitors.

In vitro studies suggest that AEA directly binds to TRPV1 and enhances capsaicin-induced calcium influx in sensory neurons derived from dorsal root ganglia [22,23] and trigeminal sensory neurons [24]. Whether such effects occur under physiological conditions is incompletely understood. However, we recently reported that genetic deletion of FAAH results in a pronociceptive phenotype in response to the TRPV1 agonist capsaicin [25]. These observations raise the possibility that high levels of AEA and/or other lipid mediators resulting from chronic FAAH inhibition, could be pronociceptive under certain conditions. It is important to note that FAAH is responsible for not only the degradation of AEA, but also several other N-acyl ethanolamines (e.g. *N*-palmitoyl ethanolamine (PEA)), endovanilloids (e.g. *N*-docosahexaenoyl ethanolamine, *N*-oleoyl ethanolamine) and arachidonic acid derivatives that do not bind to cannabinoid receptors [26]. Deletion of FAAH produces widespread changes across the lipidome in brain tissue [26], suggesting that sustained inhibition of FAAH could substantially alter the brain lipidome overall, potentially yielding unanticipated side effects.

We recently reported that both a centrally penetrant (URB597) and peripherally restricted (URB937) FAAH inhibitor, administered acutely, synergized with the opioid analgesic morphine in suppressing neuropathic pain induced by the taxane chemotherapeutic agent paclitaxel [27]. Notably, synergistic doses of these FAAH inhibitors, which enhanced the anti-allodynic effects of morphine, did not exacerbate morphine-induced slowing of gastrointestinal transit [27]. URB937 suppressed paclitaxel-induced neuropathic pain solely through a peripheral CB_1 mechanism; anti-allodynic efficacy of URB937 was blocked completely by either a peripherally restricted CB_1 antagonist (AM6545) or a global (AM251) CB_1 antagonist, but not by a CB_2 antagonist (AM630). URB597 suppressed paclitaxel-induced neuropathic pain through both CB_1 and CB_2 mechanisms; the anti-allodynic effects of URB597 were fully blocked by AM251 but only partially blocked by AM6545 or AM630. Thus, the receptor mechanisms and sites of action underlying anti-allodynic efficacy of the brain permeant and impermeant inhibitors of FAAH only partially overlap. In the present study, we used the same mouse model of paclitaxel-induced neuropathic pain to compare the impact of chronic treatment with a centrally penetrant FAAH inhibitor (URB597) [12], a peripherally restricted (URB937) FAAH inhibitor [28] and a pan-cannabinoid agonist (WIN55,212–2) on both the development and maintenance of paclitaxel-induced allodynia. We investigated whether URB597 or URB937 would prevent the development of paclitaxel-induced neuropathic pain or reverse the maintenance of already-established paclitaxel-induced painful neuropathy. We also challenged mice in each treatment regimen with the CB_1 receptor antagonist rimonabant to precipitate somatic signs of CB_1-receptor dependent withdrawal. In addition, we evaluated whether restricting treatment with either FAAH inhibitor to the period of paclitaxel dosing would suppress

paclitaxel-induced neuropathic pain in a manner that was sustained following termination of drug delivery. Lastly, we asked whether URB597 or URB937 would alter the ability of paclitaxel to reduce tumor cell line viability in both breast cancer (i.e. 4T1) and ovarian (i.e. HeyA8) tumor cell lines in vitro. Specificity of FAAH inhibitors actions in tumor cell lines was also assessed by testing the same concentrations of URB597 and URB937 on non-tumor human-derived embryonic kidney (HEK293) cells in the presence and absence of paclitaxel.

2. Materials and methods

2.1. Subjects

Adult male C57BL/6J mice (all ~12 weeks of age and weighing ~26–32 grams at the start of experiments) were purchased from Jackson Laboratory (Bar Harbor, ME). Mice were single housed in a temperature controlled facility with ad libitum access to food and water, and maintained on a 12 hour light/dark cycle (7 AM–7 PM). All experimental procedures were approved by the Bloomington Institutional Animal Care and Use committee of Indiana University and followed the guidelines of the International Association for the Study of Pain [29].

2.2. Drugs and chemicals

Paclitaxel (Tecoland Corporation, Edison, NJ, USA) was dissolved in a 1: 1: 18 ratio of cremophor EL: ethanol: saline and injected intraperitoneally (i.p.) in a volume of 6.67 mL/kg. URB597, URB937 and WIN55,212–2 (all from Cayman chemical Company, Ann Arbor, MI) and rimonabant (National Institute on Drug Abuse, Bethesda, MD) were dissolved in a vehicle consisting of 20% DMSO: 8% ethanol: 8% emulphor and 64% saline and administered via intraperitoneal (i.p.) injection in a volume of 5 mL/kg. FAAH inhibitors (URB597, URB937) were administered 2 hours prior to behavioral testing (i.e. when AEA and other fatty acid amides are validated to be elevated but 2-AG levels are unaffected) [8]. WIN55,212–2 was administered (i.p.) 30 minutes prior to behavioral testing as performed in our previous work [30].

2.3. General experimental protocol

All behavioral experiments were conducted by a single experimenter (RAS) blinded to the treatment condition. Mice were randomly assigned to experimental conditions. Animals were single housed prior to chronic dosing, which preserved blinding of the experimenter throughout drug manipulations and in vivo testing procedures and maintained continuity with our previously published work employing chronic dosing of other cannabinoid modulators (i.e. THC, CP55,940, JZL184, GAT211, AM1710 and LY2828360) in the same neuropathic pain model [27,30–35]. Videos were scored by an independent observer (SM) who was blinded to experimental conditions.

2.4. Assessment of paw withdrawal thresholds to mechanical stimulation

Paw withdrawal thresholds (in grams) to mechanical stimulation were measured using an electronic von Frey anesthesiometer (IITC model Alemo 2390–5, Woodland Hills, CA) as described previously [30,36]. Mice were placed on an elevated metal mesh table where they were habituated under individual, inverted plastic cages for at least 20 minutes prior to

testing. Following the cessation of exploratory behaviors, a force was applied to the midplantar region of the hind paw with a semi-flexible tip connected to the anesthesiometer. Mechanical stimulation was terminated when the mouse withdrew its paw from the mesh surface. The threshold for paw withdrawal was determined in duplicate in each paw; responsiveness in each paw was averaged into a single determination for each animal.

2.5. Assessment of responsivity to cold stimulation

Responsiveness to acetone was measured ~30 min following assessment of responsiveness to mechanical stimulation. Using the blunt end of a 1cc syringe, a bubble (~5–6 μL) of acetone was applied to the plantar surface of the hindpaw. The total time the animal spent elevating, shaking or licking the acetone-stimulated paw was recorded over a one minute period following application. This was repeated three times per paw, alternating stimulations between paws such that ~7 minutes separated successive applications of cutaneous stimulation to the same animal. Values were calculated as the mean of 6 stimulations (3 per paw) from each subject.

2.6. Paclitaxel-induced neuropathic pain

Paclitaxel (4 mg/kg i.p.) or its cremophor vehicle was administered once daily every other day over a 6 day period (i.e. day 0, 2, 4 and 6). In studies evaluating the maintenance of paclitaxel-induced neuropathic pain, behavioral testing occurred on day 0, 4, 7, and 15 as described previously [32,36] followed by drug treatments starting on day 16. In studies evaluating the impact of pharmacological treatments on the development of paclitaxel-induced neuropathic pain, behavioral testing took place before and on day 0, 4, 8, 16, and 20 days following initiation of paclitaxel dosing. Behavioral testing took place every 4 days following the initiation of drug treatments in each condition. In our previous work, paclitaxel treatment did alter marble burying or nestlet shredding under conditions in which allodynia was present, while our lab [30,31,36–39] and others [40–44] have shown that assessments of evoked measures of mechanical and cold hypersensitivities are reliable and reproducible dependent measures that document the existence of behavioral hypersensitivities that persist for many weeks following termination of paclitaxel dosing. Therefore, we compared the impact of chronic treatments on measures of evoked pain (i.e. to mechanical and cold stimulation) in our assessments of analgesic efficacy and tolerance. Physical dependence was assessed in the same animals by precipitating withdrawal using a CB_1 antagonist [30,32].

2.7. Comparison of FAAH inhibitors with the orthosteric cannabinoid agonist WIN55,212–2 in reversing the maintenance of paclitaxel-induced neuropathic pain

In Experiment 1, mice were treated with URB597 (1 mg/kg/day i.p.), URB937 (1 mg/kg/day i.p.) or WIN55,212–2 (3 mg/kg/day i.p.) once daily for 21 consecutive days beginning on day 16, when paclitaxel-induced hypersensitivities to mechanical and cold stimulation were already established and maintained. Behavioral testing or responsiveness to mechanical and cold stimulation was performed every 4 days.

2.8. Comparison of peripherally restricted and brain penetrant FAAH inhibitors with the orthosteric cannabinoid agonist WIN55,212–2 in suppressing the development of paclitaxel-induced neuropathic pain

In Experiment 2, URB597 (1 mg/kg/day i.p.), URB937 (1 mg/kg/ day i.p.) and WIN55,212–2 (3 mg/kg/day i.p.) were evaluated for their ability to suppress the development of paclitaxel-induced hypersensitivities. Once daily drug treatments began the same day as paclitaxel treatment, and continued for 20 days, with behavioral testing performed every 4 days.

In Experiment 3, in a separate set of animals, URB597 (1 mg/kg/day i.p.), URB937 (1 mg/kg/day i.p.) or vehicle were administered in a truncated dosing regimen (i.e. once daily for 8 days beginning on day 0) to determine whether these FAAH inhibitors would differentially alter the development of paclitaxel-induced neuropathic pain in a manner that would be sustained following termination of dosing with each inhibitor.

2.9. Evaluation of cannabinoid CB_1 receptor-mediated dependence

In studies evaluating either the maintenance (Experiment 1) or development (Experiment 2) of paclitaxel-induced neuropathic pain, all mice were given an i.p. injection of vehicle followed 30 min later by the CB_1 inverse agonist rimonabant (10 mg/kg i.p.). Vehicle challenge was used to permit evaluation of any impact of prior chronic dosing with the pharmacological treatments on intrinsic behavior. Rimonabant challenge was used to precipitate a CB_1-dependent withdrawal syndrome, if observed, that is elicited by the CB_1 antagonist [32] following chronic dosing with cannabinoid agonists in the same mice. All animals, consequently, received both challenge injections. Challenges were initiated 30 or 120 minutes after the last drug treatment with WIN55,212–2, FAAH inhibitor (i.e. URB597, URB937) or vehicle, respectively. The entire 30 min interval following each challenge injection was video-recorded and subsequently scored. The number of bouts of scratching and paw tremors were scored by a single observer blinded to treatment condition (SM) using BORIS open source software [45]. Any break in the occurrence of these repetitive behaviors was defined as the termination of a bout of scratching or paw tremors.

2.10. Cell viability assay

4T1 mouse breast cancer cells were a gift from Dr. Harikrishna Nakshatri (Indiana University School of Medicine, Indianapolis, IN) and were maintained in RPMI-1640 supplemented with 10% fetal bovine serum and 1% penicillin-streptomycin. HeyA8 human ovarian cancer cells were a gift from Dr. Kenneth Nephew (Indiana University, Bloomington IN) and were maintained in DMEM supplemented with 10% fetal bovine serum and 1% penicillin-streptomycin. HEK293 cells were a gift from Dr. Ken Mackie (Indiana University, Bloomington IN) and were maintained in DMEM supplemented with 10% fetal bovine serum and 1% penicillin-streptomycin. All the cells were kept in a 37 °C incubator equipped with 5% CO_2. Cell viability was measured through the MTT assay (by ZX) as the manufacturer instructed (Roche, Indianapolis, IN). In all cell lines, each FAAH inhibitor was plated in a dose-response matrix in the presence (or absence) of ascending concentrations of paclitaxel, to enable assessment of drug combination effects at a broad range of dose levels for each agent. Cells grown on 96 well plates seeded at a density of 3000 cells/well were

treated 24 h later in an 8 × 8 dose matrix design containing either URB597 or URB937 (0–50 μM), paclitaxel (0–500 nM) or the combination of both. Then, 10 μL MTT solution (5 mg/mL) was added to each of the wells after 72 hrs incubation. Thereafter, formazan was solubilized in 100 μl solubilization solution (SDS/HCL). The absorbance was measured at an optical density (OD) of 570 nm. Cell viability was determined by comparing the absorbance values of drug-treated cells with that of untreated control cells and plotted as % control. The results reported show quantification performed on three different experiments performed on separate days with each experiment including duplicate determinations. All in vitro data sets were normalized and subjected to a single nonlinear regression analysis to generate the EC_{50}. Data from the dose-response matrix was analyzed using both Combenefit ('Combination Benefit'; Cancer Research UK Cambridge Institute; Cambridge, UK) [46] and Synergyfinder (https://synergyfinder.fimm.fi) [47] according to three synergy reference models: the Bliss independence model, the highest single agent (HSA) model, and the Loewe additivity model, as described in our previously published work [48].

2.11. Quantitative real-time polymerase chain reaction (qRT-PCR) to analyze FAAH gene expression in 4T1 and HeyA8 tumor cell lines

Total RNA was extracted from 4T1 mouse breast cancer cells and HeyA8 human ovarian cancer cells. In brief, total RNA was isolated from 4T1 and HeyA8 cells using a TRizol (Invitrogen)/RNeasy (Qiagen) RNA mini Kit according to manufacturer's instructions. RNA (100 ng) was used in Power SYBR Green RNA to Ct 1 step kit (Applied Biosystems), with the following cycling conditions: 48 °C for 30 min, 95 °C for 10 min, and 40 cycles of 95 °C for 15 s, 60 °C for 1 min, and 72 °C for 1 min. RNA expression level was described by cycle threshold (Ct), where Ct levels are inversely proportional to the amount of target nucleic acid in the sample. FAAH relative gene expression between 4T1 and HeyA8 cell lines was normalized to that of the housekeeping gene GAPDH, and calculated via the $2^{-\Delta\Delta Ct}$ method [49]. Sequences for qRT-PCR primers are as following: FAAH sense, 5′-GCT GTG CTC TTT ACC TAC CTG-3′; FAAH anti-sense, 5′-GAA GCA TTC CTT GAG GCT CAC-3′; GAPDH sense, 5′-GGGAAGCTCACTGGCATGGC-3′; GAPDH anti-sense, 5′-GGTCCACCACCCTGTTGCT-3′.

2.12. Statistical analysis

Paw withdrawal thresholds (mechanical) and duration of acetone-evoked behavior (cold) were calculated for each paw and averaged into a single determination for each mouse for each stimulus modality. Paired *t*-tests were used to compare post-paclitaxel thresholds to baseline levels of responding within a given treatment group. Two-way repeated measures ANOVA with Bonferroni post hoc tests were used to compare drug treatments across treatment windows. A priori comparisons were also made using planned comparison and paired *t*-tests, as appropriate. In vivo data was analyzed using GraphPad Prism version 5.02 for Windows (GraphPad Software, San Diego, CA, USA, www.graphpad.com). $p < 0.05$ was considered statistically significant. For the in vitro assays of tumor cell viability, the combination response (additivity, synergy, or antagonism) was analyzed using Combenefit ('Combination Benefit'; Cancer Research UK Cambridge Institute; Cambridge, UK) [46] and Synergyfinder (https://synergyfinder.fimm.fi) [47].

The experimental combination response was compared against the expected combination response, based upon the assumption of non-interaction, using three different standard reference models: the Highest single agent (HSA) model [50], the Bliss independence model [51] and the Loewe additivity model [52]. Synergyfinder uses algorithms to generate both synergy scores and the most synergistic area scores (i.e. calculated from data derived from all experiments) that enable comparison of the effects of the combinations of either URB597 or URB937 with paclitaxel on tumor cell line viability in 4T1 and HeyA8 cells and on viability of non-tumor HEK293 cells. SynergyFinder (https://synergyfinder.fimm.fi) was, therefore, used to enable an unbiased analysis of different drug combination responses and better permit comparisons of the different reference models, which rely on different underlying assumptions (see [47] for review). In the HSA model, the synergy score calculates the excess over the highest single drug response [47]. In the Bliss model, the expected response is a multiplicative effect as if the two drugs acted independently [47]. In the Loewe model, the synergy score calculates the excess over the expected response if the two drugs were the same compound [47].

3. Results

3.1. Paclitaxel induces behavioral hypersensitivities to mechanical and cold stimulation in mice

Paclitaxel (4 mg/kg, i.p. on days 0, 2, 4, 6) lowered mechanical paw withdrawal thresholds [$F_{1,8} = 122.8$, $p < 0.0001$], mechanical thresholds changed over time [$F_{5,8} = 9.019$, $p < 0.0001$] and the interaction between treatment and time was significant [$F_{5,8} = 8.445$, $p < 0.0001$] (Fig. 1A). Paclitaxel also increased cold responsivity [$F_{1,8} = 39.00$, $p < 0.0001$], cold responsivity changed over time [$F_{5,8} = 13.34$, $p < 0.0001$] and the interaction between treatment and time was significant [$F_{5,8} = 6.686$, $p = 0.0001$] (Fig. 1B).

3.2. URB597 and URB937 but not WIN55,212–2 reverse already established paclitaxel-induced allodynia without producing tolerance

In studies evaluating the impact of FAAH inhibitors on the maintenance of neuropathic pain, mechanical hypersensitivities were already established ($p < 0.01$ vs. baseline; two-tailed paired *t*-test) prior to initiating pharmacological treatments (i.e. on day 15 following initial dosing with paclitaxel). In paclitaxel treated mice, treatment with URB597 (1 mg/kg i.p. × 20 days), URB937 (1 mg/kg i.p. × 20 days), and WIN55,212–2 (3 mg/kg i.p. × 20 days) during the maintenance of neuropathy altered mechanical thresholds [$F_{3,19} = 24.19$, $p < 0.0001$], mechanical thresholds changed over time [$F_{6,19} = 15.19$, $p < 0.0001$], and the interaction between treatment and time was significant [$F_{18,19} = 8.455$, $p < 0.0001$] (Fig. 2A). Post hoc comparisons revealed that both URB597 ($p < 0.001$ vs. vehicle for all time points) and URB937 ($p < 0.001$ vs. vehicle for all time points) reduced paclitaxel-induced hypersensitivities to mechanical stimulation throughout the entire chronic dosing period. By contrast, WIN55,212–2 initially elevated mechanical paw withdrawal thresholds relative to vehicle on day 1 ($p < 0.01$), but by day 4 of repeated dosing thresholds no longer differed from vehicle ($p > 0.05$), consistent with development of tolerance to anti-allodynic efficacy of the orthosteric agonist (Fig. 2A).

In paclitaxel-treated mice, URB597 (1 mg/kg i.p. × 20 days), URB937 (1 mg/kg i.p. × 20 days), and WIN55212–2 (3 mg/kg i.p. × 20 days) reduced cold responsiveness [$F_{3,19}$ = 100.9, $p < 0.0001$], cold responsiveness varied over time [$F_{6,19}$ = 27.63, $p < 0.0001$] and the interaction between treatment and time was significant [$F_{18,19}$ = 11.90, $p < 0.0001$] (Fig. 2B). Post hoc tests revealed that both URB597 ($p < 0.05$ vs. vehicle for all time points) and URB937 ($p < 0.001$ vs. vehicle for all time points) reduced paclitaxel-induced hypersensitivities to cold stimulation throughout the chronic dosing period whereas WIN55,212–2 only suppressed cold responsiveness relative to vehicle on day 1 ($p < 0.01$). By day 4 of repeated dosing, cold response times no longer differed between WIN55,212–2 and vehicle-treated groups ($p > 0.05$), consistent with development of tolerance to anti-allodynic efficacy of the orthosteric cannabinoid agonist (Fig. 2B).

3.3. Impact of URB597, URB937 and WIN55,212–2 on CB_1 antagonist-precipitated withdrawal

Both challenge condition [$F_{1,20}$ = 23.06, $p < 0.0001$] and drug treatment [$F_{3,20}$ = 9.461, $p < 0.0004$] impacted paw tremors and the interaction between challenge condition and treatment was significant [$F_{1,20}$ = 8.073, $p < 0.001$]. Bonferroni post hoc tests revealed that mice treated with WIN55,212–2 (3 mg/kg i.p.) exhibited more paw tremors than all other groups ($p < 0.0001$) following challenge with rimonabant. By contrast, paw tremors did not differ between groups following challenge with vehicle ($p > 0.05$ vs. all groups) (Fig. 2C).

Challenge condition altered the number of scratching bouts [$F_{1,20}$ = 57.81, $p < 0.0001$], but this behavior was not impacted by chronic drug treatment [$p = 0.1240$] and the interaction between challenge condition and treatment was not significant [$p > 0.06$] (Fig. 2D).

3.4. URB597, URB937 but not WIN55,212–2 suppress the development of paclitaxel-induced allodynia without producing tolerance

In paclitaxel-treated mice, chronic pharmacological treatments initiated just prior to the start of paclitaxel treatment altered mechanical paw withdrawal thresholds [$F_{3,25}$ = 32.52, $p < 0.0001$], mechanical thresholds changed across time [$F_{5,25}$ = 20.96, $p < 0.0001$], and the interaction between treatment and time was significant [$F_{15,25}$ = 5.519, $p < 0.0001$] (Fig. 3A). Post hoc comparisons revealed that URB597 (1 mg/kg i.p. × 20 days) ($p < 0.05$ vs. vehicle days 4 through 20), and URB937 (1 mg/kg i.p. × 20 days) ($p < 0.05$ vs. vehicle days 8 through 20), initiated prior to paclitaxel dosing, suppressed the development of paclitaxel-induced mechanical hypersensitivity throughout the chronic dosing period (i.e. until day 20). By contrast, WIN55,212–2 (3 mg/kg i.p. × 20 days) elevated mechanical paw withdrawal thresholds relative to vehicle on day 4 ($p < 0.05$), but by day 8 ($p > 0.05$) of repeated dosing, paw withdrawal thresholds were no longer elevated relative to vehicle suggesting that tolerance had developed (Fig. 3A).

In paclitaxel-treated mice, pharmacological treatments reduced cold responsiveness [$F_{3,25}$ = 32.52, $p < 0.0001$], cold response times changed across time [$F_{5,25}$ = 20.96, $p < 0.0001$], and the interaction between treatment and time was significant [$F_{15,25}$ = 5.519, $p < 0.0001$] (Fig. 3B). Post hoc comparisons revealed that URB597 (1 mg/kg i.p. × 20 days) ($p < 0.001$ vs. vehicle days 8 through 20) and URB937 (1 mg/kg i.p. × 20 days) ($p < 0.001$ vs. vehicle days

8 through 20) suppressed the development of cold hypersensitivities throughout the chronic dosing period (i.e. until day 20). By contrast, WIN55,212–2 (3 mg/kg i.p. × 20 days) initially suppressed cold responsiveness relative to vehicle on day 4 ($p < 0.05$), but by day 12 ($p > 0.05$) cold response times no longer differed from vehicle, consistent with development of tolerance (Fig. 3B).

On day 21 of chronic dosing, mice were challenged with vehicle (i.p.) followed by challenge with the CB_1 antagonist rimonabant (10 mg/kg i.p.) 30 minutes later. Challenge condition [$F_{1,20} = 21.45$, $p < 0.0001$] altered paw tremors whereas chronic treatment failed to do so [$p = 0.4158$] and the interaction between challenge condition and chronic treatment was not significant [$p = 0.4541$] (Fig. 3C).

Challenge condition [$F_{1,20} = 91.4$, $p < 0.0001$] altered the number of scratching bouts whereas chronic treatments trended to differ [$F_{3,20} = 2.992$, $p = 0.0553$], and the interaction between challenge condition and chronic treatment approached significance [$F_{1,20} = 2.599$, $p = 0.0806$]. Planned comparison *t*-tests revealed that rimonabant-induced scratching tended to be lower in groups receiving WIN55,212–2 compared to groups receiving vehicle ($p = 0.0539$, one tailed *t*-test) (Fig. 3D).

3.5. URB597 or URB937 does not prevent the development of paclitaxel-induced hypersensitivities

In paclitaxel-treated mice, restricted dosing with either URB597 (1 mg/kg i.p. × 8 days) or URB937 (1 mg/kg i.p. × 8 days) during the development of neuropathy altered mechanical responding in a time dependent manner, as documented by a significant interaction between treatment and time [$F_{10,15} = 4.331$, $p < 0.0001$], mechanical responding changed over time [$F_{2,15} = 105.3$, $p < 0.0001$], and the main effect of chronic treatment was not significant [$F_{2,15} = 1.273$, $p > 0.05$] (Fig. 4A). Post hoc tests revealed that both URB937 (day 8: $p < 0.05$) and URB597 (day 4: $p < 0.05$; day 8: $p < 0.01$) elevated mechanical paw withdrawal thresholds relative to vehicle at specific time points (Fig. 4A).

In paclitaxel-treated mice, restricted 8-day dosing with either URB597 or URB937 during the development of paclitaxel neuropathy attenuated cold responsiveness [$F_{2,15} = 10.15$, $p < 0.0001$], cold responsiveness changed across time [$F_{2,15} = 116.7$, $p < 0.0001$], and the interaction between chronic treatment and time was significant [$F_{10,15} = 4.713$, $p < 0.0001$]. Post hoc comparisons revealed that URB597 ($p < 0.05$ vs. vehicle day 4 and 8) and URB937 ($p < 0.05$ vs. vehicle day 4, 8 and 16) (Fig. 4B) suppressed the development of cold hypersensitivities. Neither treatment was able to permanently prevent paclitaxel-induced hypersensitivities from developing.

3.6. Impact of FAAH inhibitor in the presence and absence of paclitaxel on breast and ovarian tumor cell line viability

We examined the impact of URB597 (see Figs. 5 and 7), URB937 (see Figs. 6 and 8) and paclitaxel (Figs. 5–8) over a wide range of molar ratios (i.e. dose-response matrix between 8 concentrations of the FAAH inhibitor and 8 concentrations of paclitaxel) on 4T1 (Figs. 5 and 6) and HeyA8 (Figs. 7 and 8) tumor cell line viability. As expected, paclitaxel reduced tumor cell line viability (% control) in both 4T1 (Figs. 5A and 6A) and HeyA8 cells (Figs. 7A and

8A). The EC_{50} for paclitaxel in reducing tumor cell line viability ranged from 12.1 nM (Fig. 5A) to 16.3 nM (Fig. 6A) in 4T1 cells and between 6.41 nM (Fig. 7A) to 8.41 nM (Fig. 8A) in HeyA8 cells. Both URB597 (EC_{50} = 32.6 μM, Fig. 5B) and URB937 (EC_{50} = 16.7 μM, Fig. 6B) inhibited 4T1 tumor cell viability in the absence of paclitaxel.

The impact of various concentrations of URB597 (Figs. 5C and 7C) and URB937 (Figs. 6C and 8C) on the dose response curve for paclitaxel in suppressing tumor cell line viability is shown for 4T1 (Figs. 5C and 6C) and HeyA8 (Figs. 7C and 8C) cell lines. Similarly, the impact of various concentrations of paclitaxel (Figs. 5D, 6D, 7D and 8D) on the dose response curve for either URB597 (Figs. 5D and 7D) or URB937 (Figs. 6D and 8D) to alter tumor cell line viability is shown for 4T1 (Figs. 5D and 6D) and HeyA8 (Figs. 7D and 8D) cell lines, respectively. Computational quantification of the drug combination responses, plotted as a three dimensional synergy map over the dose matrix, indicate that the combination of FAAH inhibitor with paclitaxel in 4T1 cells is synergistic using the Bliss model (4T1: Figs. 5E, 6E and Table 1), HSA model (Figs. 5F, 6F and Table 1), and Loewe Additivity model (Figs. 5G, 6G, and Table 1). By contrast, the FAAH inhibitors alone had no or minimal effects on viability in HeyA8 (EC_{50} > 100 μM for URB597 (Fig. 7B) and EC_{50} = 388 μM for URB937 (Fig. 8B)) tumor cells, which was markedly inhibited by paclitaxel in each case (Figs. 7A and 8A).

The color-coded three dimensional synergy map, plotted over the dose matrix, indicate that the combination of FAAH inhibitors and paclitaxel in HeyA8 cells is synergistic using the Bliss model (Figs. 7E, 8E and Table 1), HSA model (Figs. 7F, 8F and Table 1), and Loewe Additivity model (Figs. 7G, 8G, and Table 1). The synergy maps show that FAAH inhibitors in combination with paclitaxel have synergistic effects (blue areas in the model graph) in inhibiting tumor cell viability at a wide range of drug combination ratios in both 4T1 (Figs. 5E–G and 6E–G) cells and HeyA8 (Figs. 7E–G and 8E–G) tumor cell lines.

To rule out the possibility that nonspecific cytotoxicity was induced by our manipulations, we also examined the impact of URB597 or URB937, in the presence and absence of paclitaxel, on viability of non-tumor HEK293 cells using the same dose matrix analyses and computational approach. Paclitaxel showed limited efficacy (EC_{50} > 500 nM) in reducing cell viability of HEK293 (Figs. 9A and 10A) cells, in contrast to observations of robust reductions in cell viability produced by paclitaxel in either 4T1 (Figs. 5A and 6A) cells or HeyA8 (Figs. 7A and 8A) cells. Neither URB597 (Fig. 9B) nor URB937 (Fig. 10B) altered HEK293 cell viability. Lack of effect of various concentrations of URB597 (Fig. 9C) and URB937 (Fig. 10C) on the dose response of paclitaxel on HEK293 cell line viability is shown by linear dose response curves observed in each case. Similarly, the relative lack of effect of various concentrations of paclitaxel (Figs. 9D and 10D) on the dose response of either URB597 (Fig. 9D) or URB937 (Fig. 10D) on HEK293 cell line viability is shown by linear dose response curves observed in each case. The three dimensional synergy maps, plotted over the dose matrix, indicate that, in HEK293 cells, the combination of either URB597 (Fig. 9E–G) or URB937 (Fig. 10E–G) with paclitaxel was either antagonistic or neutral in its impact on cell viability according to the Bliss model (Figs. 9E, 10E), HSA model (Figs. 9F and 10F) or Loewe Additivity model (Figs. 9G and 10G).

In both 4T1 and HeyA8 cells, the combinations of either FAAH inhibitor with paclitaxel were synergistic in the tumor cell lines, based upon observations of positive synergy scores and most synergistic area scores for these combinations, as calculated by Synergyfinder (Table 1). Assessment of synergy scores and most synergistic area scores revealed that, in combination with paclitaxel, URB597 was more synergistic than URB937 in reducing 4T1 tumor cell line viability, whereas the effects of the two FAAH inhibitors were more comparable in HeyA8 cells (Table 1). By contrast, in HEK293 cells, Synergyfinder failed to reveal evidence of synergy of FAAH inhibitors in combination with paclitaxel in altering viability of non-tumor cells. In fact, in HEK293 cells, synergy scores and most synergistic areas scores were negative or neutral for either URB597 or URB937 in combination with paclitaxel (Table 1).

3.7. 4T1 and HeyA8 cells express FAAH mRNA

qRT-PCR experiments verified that both 4T1 and HeyA8 cell lines used in these experiments express FAAH mRNA. FAAH mRNA in each sample was normalized to GAPDH mRNA that corresponded to the same sample. The mean ΔCt value was 9.813 ± 1.24 for 4T1 and 11.25 ± 0.17 for HeyA8 cell lines, respectively. In 4T1 tumor cells, the mean Ct value for GAPDH was 16.29 ± 0.67, whereas the mean Ct value for FAAH was 26.11 ± 0.05, indicating that FAAH mRNA is abundantly expressed in 4T1 cell lines. In HeyA8 tumor cell lines, the mean Ct value for GAPDH was 21.08 ± 0.23, whereas the mean CT value for FAAH was 32.33 ± 0.18, indicating that the HeyA8 cell line has a moderate amount of FAAH gene expression. Relative FAAH mRNA expression in 4T1 cells was 2.7 fold of the level expressed in HeyA8 cells using $2^{-\Delta\Delta Ct}$ method.

4. Discussion

A number of clinical trial failings of FAAH inhibitors [17–19] suggest the importance of better understanding the relationship between FAAH inhibition and different pain pathologies to optimize potential for clinical translation of pain therapeutics. Inhibition of FAAH is efficacious in a number of different preclinical neuropathic pain models [53,54] (e.g. chronic constriction injury (CCI) [55–57], partial sciatic nerve ligation (PSNL) [16], spinal nerve ligation (SNL) (rat) [58], and chemotherapy-induced peripheral neuropathy [8]). Importantly, FAAH inhibitors lack unwanted pharmacological effects associated with direct CB_1 receptor activation (i.e. tolerance, dependence, catalepsy). The present study supports and extends this body of literature, providing evidence that peripheral and central inhibition of FAAH reduces both the development and maintenance of paclitaxel-induced neuropathic pain without the occurrence of cannabinoid CB_1 receptor-mediated physical dependence or tolerance. In our study, anti-allodynic efficacy was sustained over a chronic dosing period of 20 days with either inhibitor, although neuropathic pain was not permanently prevented in a restricted prophylactic dosing paradigm.

Inhibitors of FAAH, administered acutely, are efficacious in suppressing chemotherapy-induced neuropathic pain in rodents [8,59], but our study is the first to evaluate inhibitors of FAAH that differ in their ability to penetrate the CNS for possible signs of tolerance or physical dependence in a model of chemotherapy-induced neuropathy (CIPN). Moreover,

efficacy of brain permeant and impermeant FAAH inhibitors on the development of neuropathic pain has not previously been compared using prophylactic and therapeutic dosing paradigms. We report that both URB597 and URB937 suppressed both the development and maintenance of paclitaxel-induced hypersensitivities to mechanical and cold allodynia over a 20-day chronic dosing period. This observation is in contrast to the orthosteric pan-cannabinoid agonist WIN55,212–2, which initially suppressed paclitaxel-induced behavioral hypersensitivities but was no longer effective in producing antinociception by day 8 of repeated dosing. This observation suggests that inhibition of FAAH, and peripheral FAAH inhibition only, may be superior to exogenous administration of cannabinoid agonists in reducing allodynia during the development paclitaxel-induced neuropathic pain. Sasso and colleagues previously reported that both URB597 and URB937, administered acutely, suppress inflammatory pain due to carrageenan and complete Freund's adjuvant inflammation of the hindpaw as well as neuropathic pain due to chronic sciatic nerve ligation [60]. However, in this latter study, URB937 was more effective than global FAAH inhibitors (URB597, PF-04457845) in suppressing inflammatory pain [60]. Interestingly, in our study URB597 and URB937 were equally effective in suppressing both the development and maintenance of paclitaxel-induced neuropathic pain. More work is necessary to determine whether FAAH inhibitors would be efficacious in suppressing chemotherapy-induced neuropathic pain in people.

We restricted pharmacological manipulations to the interval associated with paclitaxel dosing to examine whether anti-allodynic effects of either FAAH inhibitor would outlast the period of drug delivery and permanently prevent expression of paclitaxel-induced neuropathic pain. When administered over this truncated 8-day period, URB597 and URB937 delayed the onset of, but did not fully prevent, development of paclitaxel-induced neuropathic pain. Thus, inhibition of FAAH during the development of paclitaxel-induced neuropathy is not sufficient to prevent pathological changes initiated by paclitaxel that produce allodynia. This observation may reflect limited duration of action of the inhibitors given by i.p. injection. For example, chronic infusion of CB_2 or mixed CB_1/CB_2 agonists (i.e. AM1710, WIN55,212–2) results in a long-lasting prevention of paclitaxel-induced hypersensitivity that outlasted the period of drug delivery by approximately two weeks [61,62]. However, neuropathic pain eventually returned following termination of these chronic infusions [61,62]. In our previous reports, URB597 produced anti-allodynic properties in suppressing chemotherapy-induced neuropathic pain through CB_1 and CB_2 receptor mechanisms [63]. By contrast, peripheral CB_1 receptor activation underlies URB937's efficacy in this model and in a CCI model of traumatic nerve injury [64]. FAAH inhibition indirectly activates CB_1 receptors by elevating levels of endogenous AEA (along with other fatty-acid amides) but is not sufficient to prevent paclitaxel-induced hypersensitivities from developing [42]. Our lab has previously reported no change in FAAH mRNA levels in the spinal cord of mice [32] following paclitaxel (4 mg/kg i.p. every other day 4 days) treatment. Similarly, paclitaxel (8 mg/kg i.p. every other day 4 days) did not change whole brain or spinal cord endocannabinoid levels or CB_1/CB_2 receptor mRNA in mice [42]. Thus, targeting the endocannabinoid system alone is likely not sufficient to prevent pathological alterations ultimately resulting in allodynia following the onset of paclitaxel treatment.

Akin to our findings in the development phase of paclitaxel-induced allodynia, URB597 and URB937 abrogated already established paclitaxel-induced allodynia without the development of tolerance (i.e. when administered once daily over a 20 day dosing period). By contrast, WIN55,212–2 initially reversed already established paclitaxel-induced allodynia, but tolerance developed after 4 days of repeated dosing. This observation is consistent with previous reports showing that direct cannabinoid agonists such as Δ^9-THC [32] and CP55,940 [31] suppress paclitaxel-induced allodynia initially but lose efficacy following repeated daily dosing. Thus, FAAH inhibition, and specifically peripheral FAAH inhibition, is sufficient to suppress already established paclitaxel-induced allodynia without development of tolerance, in contrast to the robust development of tolerance observed with orthosteric cannabinoid CB_1 agonists [30–32].

In mice treated with WIN55,212–2 during the maintenance phase of paclitaxel-induced neuropathy, rimonabant challenge elicited more bouts of paw tremors than any other group, consistent with an unmasking of CB_1-dependent withdrawal symptoms. This is in line with previous findings from our lab [32,33] and others [65–67] showing that a CB_1 antagonist precipitates somatic withdrawal behaviors in mice treated chronically with a CB_1 agonist. Interestingly, rimonabant-precipitated withdrawal may be less pronounced in animals treated during the development phase of paclitaxel-induced allodynia relative to mice receiving the same cannabinoid agonist treatment in the maintenance phase. CB_1 desensitization or downregulation following chronic WIN55,212–2 treatment could potentially contribute to differences between the studies. While others have reported no change in whole-brain CB_1 receptor levels following paclitaxel treatment [42] during the maintenance phase of neuropathy, CB_1 receptor density or efficacy could differ in distinct regions that are involved with the somatic expression of withdrawal (e.g. locus coeruleus) [68]. More work is necessary to fully understand this relationship.

Rimonabant itself induces a pruritic response associated with scratching that is mediated by CB_1, as evidenced by the fact that rimonabant-induced scratching is absent in CB_1 KO mice [69]. Thus, it is noteworthy that neither URB597, URB937 nor WIN55,212–2 altered rimonabant-induced scratching in our study. URB597, administered acutely, can suppress rimonabant-induced scratching behavior, although the dose of URB597 employed in that study was much higher (10 mg/kg i.p.) and the dose of rimonabant employed was much lower (1 mg/kg i.p.) than the doses used in the present studies [70]. Rimonabant-induced scratching is also attenuated by acute treatment with WIN55,212–2 [71]. We did, however, observe lower levels of rimonabant-induced scratching under conditions in which paw tremors, a wellvalidated measure of cannabinoid CB_1-mediated withdrawal [6,31,32,65,72,73], were also increased by rimonabant challenge. This observation is likely due to the fact that paw tremors and scratching bouts are temporally distinct behaviors that do not occur simultaneously.

Strikingly, peripheral FAAH inhibition alone was sufficient to suppress the development of and reverse already-established paclitaxel-induced allodynia. We have previously reported that anti-allodynic effects of URB937, administered acutely, are mediated by peripheral CB_1 receptors only [63]. This is in line with previous reports using other pain models [64] that peripheral CB_1 receptor activation is sufficient to elicit anti-allodynic effects [74]. However,

PPARα receptors are involved in the anti-allodynic effects of PEA, another fatty-acid amide which is also degraded by FAAH and elevated following its inhibition [41,75], thus potential contributions from these receptors to observed in vivo effects cannot be ruled out.

Importantly, our studies demonstrate that neither URB597 nor URB937 impeded the anti-tumor efficacy of paclitaxel in breast (4T1) and ovarian (HeyA8) tumor cell lines. In fact, the FAAH inhibitors, by themselves, reduced 4T1 tumor cell line viability, albeit with low potency, but largely lacked intrinsic efficacy in reducing HeyA8 tumor cell line viability. Nonetheless, computational quantification of the dose matrix of the combination of each FAAH inhibitor with paclitaxel showed evidence for synergism in reducing tumor cell line viability in our analyses using three different synergy models: the Bliss model, the Highest Single Agent (HSA) model and the Loewe model. Moreover, the same conclusions were derived from computational quantification of the dose matrix of the combination responses from tumor cell viability assays performed using both 4T1 and HeyA8 cells. URB597 was also associated with higher synergy and greatest synergistic area scores relative to URB937 in breast cancer (4T1) cell lines. Importantly, the synergistic effects of FAAH inhibitors in enhancing tumor cell line viability cannot be attributed to non-specific cytotoxic effects. As expected, paclitaxel showed very limited efficacy in reducing viability of HEK293 cells, which was not inhibited by URB597 or URB937, and the combination of either FAAH inhibitor with paclitaxel also failed to inhibit viability of non-tumor cells. These observation suggest that the FAAH inhibitors preferentially increase cytotoxic effects of paclitaxel in reducing tumor cell line viability without reducing viability of normal non-tumor cells. These observations document differential sensitivity of the target cancer cell type compared to normal cells when treated with the same combinations of FAAH inhibitor and paclitaxel. Of course, caution must be exerted in extrapolating results from in vitro studies to the in vivo condition.

It is possible that the modest intrinsic effect of FAAH inhibitors in reducing 4T1 but not HeyA8 tumor cell line cytotoxicity in the absence of paclitaxel relates to higher expression levels of FAAH mRNA in 4T1 compared to HeyA8 tumor cell lines. Notably, differences in FAAH mRNA expression levels cannot be attributed to differences in levels of the housekeeping gene GAPDH in the two different cell lines. The results of these experiments, nonetheless, support our hypothesis that prophylactic treatment with FAAH inhibitors would be unlikely to interfere with the anti-tumor efficacy of paclitaxel in ovarian and breast cancer patients receiving FAAH inhibitors during chemotherapy treatment, and could potentially be beneficial as adjunctive strategies. Interestingly, URB597 reduces melanoma (B16) [76] and mouse neuroblastoma (N1E-115) [77] cell viability and the FAAH inhibitor PF-3845 reduces human colon cancer cell (Colo-205) viability [78], further suggesting that FAAH inhibition is unlikely to impede, and may actually enhance, the impact of chemotherapeutic agents on tumor cell cytotoxicity. Such an interpretation is consistent with the results of in vitro assay of tumor cell line viability performed here. More work is necessary to determine whether the present in vitro findings showing synergistic effect of FAAH inhibitors in reducing tumor cell line viability translate to in vivo studies in tumor-bearing animals. Our in vivo studies, therefore, support the hypothesis that FAAH inhibitors could be useful as adjunctive analgesic strategy for suppressing chemotherapy-induced neuropathic pain in cancer patients.

In conclusion, our results verify an important therapeutic application for FAAH inhibitors in suppressing neuropathic pain due to chemotherapeutic treatment with paclitaxel. Moreover, FAAH inhibition is likely to represent a superior therapeutic strategy for suppressing paclitaxel-induced neuropathic pain relative to direct targeting of orthosteric CB_1 receptor binding sites; both a brain permeant (URB597) and a brain impermeant (URB937) inhibitor of FAAH suppressed both the development and maintenance of paclitaxel-induced neuropathic pain without producing either tolerance or cannabinoid CB_1-mediated physical dependence. Moreover, neither URB597 nor URB937 impeded the ability of paclitaxel to produce tumor cell line cytotoxicity in either breast cancer (4T1) or ovarian cancer (HeyA8) tumor cell lines. Finally, the combination of FAAH inhibitors with paclitaxel showed evidence for synergism in reducing tumor cell line viability in both 4T1 and HeyA8 tumor cell lines. Our results collectively suggest that FAAH inhibition may be therapeutically beneficial in patients that exhibit CIPN and that further clinical trials for this indication are warranted.

Acknowledgments

Supported by DA041229, DA009158 and CA200417 (to AGH). RAS was supported by NIDA T32 training grant DA024628.

References

[1]. Woodhams SG, et al., The cannabinoid system and pain, Neuropharmacology 124 (2017) 105–120. [PubMed: 28625720]

[2]. Rahn EJ, Hohmann AG, Cannabinoids as pharmacotherapies for neuropathic pain: from the bench to the bedside, Neurotherapeutics 6 (4) (2009) 713–737. [PubMed: 19789075]

[3]. Adams IB, Compton DR, Martin BR, Assessment of anandamide interaction with the cannabinoid brain receptor: SR 141716A antagonism studies in mice and autoradiographic analysis of receptor binding in rat brain, J. Pharmacol. Exp. Ther 284 (3) (1998) 1209–1217. [PubMed: 9495885]

[4]. Zoratti C, et al., Anandamide initiates Ca(2+) signaling via CB2 receptor linked to phospholipase C in calf pulmonary endothelial cells, Br. J. Pharmacol 140 (8) (2003) 1351–1362. [PubMed: 14645143]

[5]. Pertwee RG, et al., International Union of Basic and Clinical Pharmacology. LXXIX. Cannabinoid receptors and their ligands: beyond CB(1) and CB(2), Pharmacol. Rev 62 (4) (2010) 588–631. [PubMed: 21079038]

[6]. Schlosburg JE, et al., Chronic monoacylglycerol lipase blockade causes functional antagonism of the endocannabinoid system, Nat. Neurosci 13 (9) (2010) 1113–1119. [PubMed: 20729846]

[7]. Kinsey SG, et al., Repeated low-dose administration of the monoacylglycerol lipase inhibitor JZL184 retains cannabinoid receptor type 1-mediated antinociceptive and gastroprotective effects, J. Pharmacol. Exp. Ther 345 (3) (2013) 492–501. [PubMed: 23412396]

[8]. Guindon J, et al., Alterations in endocannabinoid tone following chemotherapy-induced peripheral neuropathy: effects of endocannabinoid deactivation inhibitors targeting fatty-acid amide hydrolase and monoacylglycerol lipase in comparison to reference analgesics following cisplatin treatment, Pharmacol. Res 67 (1) (2013) 94–109. [PubMed: 23127915]

[9]. Khasabova IA, et al., Cannabinoid type-1 receptor reduces pain and neurotoxicity produced by chemotherapy, J. Neurosci 32 (20) (2012) 7091–7101. [PubMed: 22593077]

[10]. Parker LA, et al., A comparison of novel, selective fatty acid amide hydrolase (FAAH), monoacylglycerol lipase (MAGL) or dual FAAH/MAGL inhibitors to suppress acute and anticipatory nausea in rat models, Psychopharmacology (Berl) 233 (12) (2016) 2265–2275. [PubMed: 27048155]

[11]. Hill MN, Gorzalka BB, The endocannabinoid system and the treatment of mood and anxiety disorders, CNS Neurol. Disord. Drug Targets 8 (6) (2009) 451–458. [PubMed: 19839936]

[12]. Kathuria S, et al., Modulation of anxiety through blockade of anandamide hydrolysis, Nat. Med 9 (1) (2003) 76–81. [PubMed: 12461523]

[13]. Schlosburg JE, et al., Inhibitors of endocannabinoid-metabolizing enzymes reduce precipitated withdrawal responses in THC-dependent mice, AAPS J. 11 (2) (2009) 342–352. [PubMed: 19430909]

[14]. Cravatt BF, et al., Chemical characterization of a family of brain lipids that induce sleep, Science 268 (5216) (1995) 1506–1509. [PubMed: 7770779]

[15]. Naidu PS, et al., Evaluation of fatty acid amide hydrolase inhibition in murine models of emotionality, Psychopharmacology (Berl) 192 (1) (2007) 61–70. [PubMed: 17279376]

[16]. Desroches J, et al., Endocannabinoids decrease neuropathic pain-related behavior in mice through the activation of one or both peripheral CB(1) and CB(2) receptors, Neuropharmacology 77 (2014) 441–452. [PubMed: 24148808]

[17]. Huggins JP, et al., An efficient randomised, placebo-controlled clinical trial with the irreversible fatty acid amide hydrolase-1 inhibitor PF-04457845, which modulates endocannabinoids but fails to induce effective analgesia in patients with pain due to osteoarthritis of the knee, Pain 153 (9) (2012) 1837–1846. [PubMed: 22727500]

[18]. Bradford D, et al., The MOBILE Study—a phase IIa enriched enrollment randomized withdrawal trial to assess the analgesic efficacy and safety of ASP8477, a fatty acid amide hydrolase inhibitor, in patients with peripheral neuropathic pain, Pain Med. 18 (12) (2017) 2388–2400. [PubMed: 28383710]

[19]. Wagenlehner FME, et al., Fatty acid amide hydrolase inhibitor treatment in men with chronic prostatitis/chronic pelvic pain syndrome: an adaptive double-blind, randomized controlled trial, Urology 103 (2017) 191–197. [PubMed: 28254462]

[20]. Moore N, Lessons from the fatal French study BIA-10–2474, BMJ 353 (2016) i2727. [PubMed: 27193592]

[21]. van Esbroeck ACM, et al., Activity-based protein profiling reveals off-target proteins of the FAAH inhibitor BIA 10–2474, Science 356 (6342) (2017) 1084–1087. [PubMed: 28596366]

[22]. Olah Z, Karai L, Iadarola MJ, Anandamide activates vanilloid receptor 1 (VR1) at acidic pH in dorsal root ganglia neurons and cells ectopically expressing VR1, J. Biol. Chem 276 (33) (2001) 31163–31170. [PubMed: 11333266]

[23]. Chen J, et al., Spatial distribution of the cannabinoid type 1 and capsaicin receptors may contribute to the complexity of their crosstalk, Sci. Rep 6 (2016) 33307. [PubMed: 27653550]

[24]. Roberts LA, Christie MJ, Connor M, Anandamide is a partial agonist at native vanilloid receptors in acutely isolated mouse trigeminal sensory neurons, Br. J. Pharmacol 137 (4) (2002) 421–428. [PubMed: 12359623]

[25]. Carey LM, et al., A pro-nociceptive phenotype unmasked in mice lacking fatty-acid amide hydrolase, Mol. Pain 12 (2016).

[26]. Leishman E, et al., Broad impact of deleting endogenous cannabinoid hydrolyzing enzymes and the CB1 cannabinoid receptor on the endogenous cannabinoid-related lipidome in eight regions of the mouse brain, Pharmacol. Res 110 (2016) 159–172. [PubMed: 27109320]

[27]. Slivicki RA, et al., Brain-permeant and -impermeant inhibitors of fatty acid amide hydrolase synergize with the opioid analgesic morphine to suppress chemotherapy-induced neuropathic nociception without enhancing effects of morphine on gastrointestinal transit, J. Pharmacol. Exp. Ther 367 (3) (2018) 551–563. [PubMed: 30275151]

[28]. Moreno-Sanz G, et al., The ABC membrane transporter ABCG2 prevents access of FAAH inhibitor URB937 to the central nervous system, Pharmacol. Res 64 (4) (2011) 359–363. [PubMed: 21767647]

[29]. Zimmermann M, Ethical guidelines for investigations of experimental pain in conscious animals, Pain 16 (2) (1983) 109–110. [PubMed: 6877845]

[30]. Slivicki RA, et al., Positive allosteric modulation of cannabinoid receptor type 1 suppresses pathological pain without producing tolerance or dependence, Biol. Psychiatry 84 (10) (2017) 722–733. [PubMed: 28823711]

[31]. Deng L, et al., CB1 knockout mice unveil sustained CB2-mediated antiallodynic effects of the mixed CB1/CB2 agonist CP55,940 in a mouse model of paclitaxel-induced neuropathic pain, Mol. Pharmacol 88 (1) (2015) 64–74. [PubMed: 25904556]

[32]. Deng L, et al., Chronic cannabinoid receptor 2 activation reverses paclitaxel neuropathy without tolerance or cannabinoid receptor 1-dependent withdrawal, Biol. Psychiatry 77 (5) (2015) 475–487. [PubMed: 24853387]

[33]. Li AL, et al., Cannabinoid CB2 agonist GW405833 suppresses inflammatory and neuropathic pain through a CB1 mechanism that is independent of CB2 receptors in mice, J. Pharmacol. Exp. Ther 362 (2) (2017) 296–305. [PubMed: 28592614]

[34]. Li AL, et al., The cannabinoid CB2 agonist AM1710 differentially suppresses distinct pathological pain states and attenuates morphine tolerance and withdrawal, Mol. Pharmacol 95 (2) (2018) 155–168. [PubMed: 30504240]

[35]. Lin X, et al., Slowly signaling G protein-biased CB2 cannabinoid receptor agonist LY2828360 suppresses neuropathic pain with sustained efficacy and attenuates morphine tolerance and dependence, Mol. Pharmacol 93 (2) (2018) 49–62. [PubMed: 29192123]

[36]. Slivicki RA, et al., Impact of genetic reduction of NMNAT2 on chemotherapy-induced losses in cell viability in vitro and peripheral neuropathy in vivo, PLOS One 11 (1) (2016) e0147620. [PubMed: 26808812]

[37]. Deng L, et al., Prophylactic treatment with the tricyclic antidepressant desipramine prevents development of paclitaxel-induced neuropathic pain through activation of endogenous analgesic systems, Pharmacol. Res 114 (2016) 75–89. [PubMed: 27773824]

[38]. Carey LM, et al., Inflammatory and neuropathic nociception is preserved in GPR55 knockout mice, Sci. Rep 7 (1) (2017) 944. [PubMed: 28428628]

[39]. Lee WH, et al., Small molecule inhibitors of PSD95-nNOS protein-protein interactions as novel analgesics, Neuropharmacology 97 (2015) 464–475. [PubMed: 26071110]

[40]. Toma W, et al., Effects of paclitaxel on the development of neuropathy and affective behaviors in the mouse, Neuropharmacology 117 (2017) 305–315. [PubMed: 28237807]

[41]. Donvito G, et al., Palmitoylethanolamide reverses paclitaxel-induced allodynia in mice, J. Pharmacol. Exp. Ther 359 (2) (2016) 310–318. [PubMed: 27608657]

[42]. Curry Z, et al., Monoacylglycerol lipase inhibitors reverse paclitaxel-induced nociceptive behavior and proinflammatory markers in a mouse model of chemotherapy-induced neuropathy, J. Pharmacol. Exp. Ther 366 (1) (2018) 169–183. [PubMed: 29540562]

[43]. Ward SJ, et al., Cannabidiol inhibits paclitaxel-induced neuropathic pain through 5-HT(1A) receptors without diminishing nervous system function or chemotherapy efficacy, Br. J. Pharmacol 171 (3) (2014) 636–645. [PubMed: 24117398]

[44]. Ward SJ, et al., Cannabidiol prevents the development of cold and mechanical allodynia in paclitaxel-treated female C57Bl6 mice, Anesth. Analg 113 (4) (2011) 947–950. [PubMed: 21737705]

[45]. Friard O, Gamba M, BORIS: a free, versatile open-source event-logging software for video/audio coding and live observations, Methods Ecol. Evol 7 (11) (2016) 1325–1330.

[46]. Di Veroli GY, et al., Combenefit: an interactive platform for the analysis and visualization of drug combinations, Bioinformatics 32 (18) (2016) 2866–2868. [PubMed: 27153664]

[47]. Ianevski A, et al., SynergyFinder: a web application for analyzing drug combination dose-response matrix data, Bioinformatics 33 (15) (2017) 2413–2415. [PubMed: 28379339]

[48]. Lee WH, C. L.M, Li L, Xu Z, Lai Y, Courtney MJ, Hohmann AG, ZLc002, a putative small molecule inhibitor of nNOS interaction with NOS1AP, suppresses inflammatory nociception and chemotherapy-induced neuropathic pain and synergizes with paclitaxel to reduce tumor cell viability, Mol. Pain 14 (2018) 1744806918801224. [PubMed: 30157705]

[49]. Livak KJ, Schmittgen TD, Analysis of relative gene expression data using real-time quantitative PCR and the 2(-Delta Delta C(T)) Method, Methods 25 (4) (2001) 402–408. [PubMed: 11846609]

[50]. Berenbaum MC, What is synergy? Pharmacol. Rev 41 (2) (1989) 93–141. [PubMed: 2692037]

[51]. Bliss CI, The toxicity of poisons applied jointly, Ann. Appl. Biol 26 (3) (1939) 585–615.

[52]. Loewe S, The problem of synergism and antagonism of combined drugs, Arzneimittelforschung. 3 (6) (1953) 285–290. [PubMed: 13081480]

[53]. Zubrzycki M, et al., Effects of centrally administered endocannabinoids and opioids on orofacial pain perception in rats, Br. J. Pharmacol 174 (21) (2017) 3780–3789. [PubMed: 28771697]

[54]. Chundi V, et al., Biochanin-A attenuates neuropathic pain in diabetic rats, J. Ayurveda Integr. Med 7 (4) (2016) 231–237. [PubMed: 27890700]

[55]. Kinsey SG, et al., Blockade of endocannabinoid-degrading enzymes attenuates neuropathic pain, J. Pharmacol. Exp. Ther 330 (3) (2009) 902–910. [PubMed: 19502530]

[56]. Kinsey SG, et al., Fatty acid amide hydrolase and monoacylglycerol lipase inhibitors produce anti-allodynic effects in mice through distinct cannabinoid receptor mechanisms, J. Pain 11 (12) (2010) 1420–1428. [PubMed: 20554481]

[57]. Russo R, et al., The fatty acid amide hydrolase inhibitor URB597 (cyclohexylcarbamic acid 3′-carbamoylbiphenyl-3-yl ester) reduces neuropathic pain after oral administration in mice, J. Pharmacol. Exp. Ther 322 (1) (2007) 236–242. [PubMed: 17412883]

[58]. Chang L, et al., Inhibition of fatty acid amide hydrolase produces analgesia by multiple mechanisms, Br. J. Pharmacol 148 (1) (2006) 102–113. [PubMed: 16501580]

[59]. Uhelski ML, Khasabova IA, Simone DA, Inhibition of anandamide hydrolysis attenuates nociceptor sensitization in a murine model of chemotherapy-induced peripheral neuropathy, J. Neurophysiol 113 (5) (2015) 1501–1510. [PubMed: 25505113]

[60]. Sasso O, et al., Peripheral FAAH inhibition causes profound antinociception and protects against indomethacin-induced gastric lesions, Pharmacol. Res 65 (5) (2012) 553–563. [PubMed: 22420940]

[61]. Rahn EJ, et al., Prophylactic cannabinoid administration blocks the development of paclitaxel-induced neuropathic nociception during analgesic treatment and following cessation of drug delivery, Mol. Pain 10 (2014) 27. [PubMed: 24742127]

[62]. Rahn EJ, et al., Selective activation of cannabinoid CB2 receptors suppresses neuropathic nociception induced by treatment with the chemotherapeutic agent paclitaxel in rats, J. Pharmacol. Exp. Ther 327 (2) (2008) 584–591. [PubMed: 18664590]

[63]. Slivicki RA, Mali SM, Hohmann AG, Comparison of brain permeant and impermeant inhibitors of fatty-acid amide hydrolase (FAAH) with the opioid analgesic morphine on the development and maintenance of paclitaxel-induced peripheral neuropathy, Society for Neuroscience 2017, Washington, DC (2017).

[64]. Clapper JR, et al., Anandamide suppresses pain initiation through a peripheral endocannabinoid mechanism, Nat. Neurosci 13 (10) (2010) 1265–1270. [PubMed: 20852626]

[65]. Cook SA, Lowe JA, Martin BR, CB1 receptor antagonist precipitates withdrawal in mice exposed to Delta9-tetrahydrocannabinol, J. Pharmacol. Exp. Ther 285 (3) (1998) 1150–1156. [PubMed: 9618417]

[66]. Lichtman AH, Fisher J, Martin BR, Precipitated cannabinoid withdrawal is reversed by Delta(9)-tetrahydrocannabinol or clonidine, Pharmacol. Biochem. Behav 69 (1–2) (2001) 181–188. [PubMed: 11420084]

[67]. Tai S, et al., Cannabinoid withdrawal in mice: inverse agonist vs neutral antagonist, Psychopharmacology (Berl) 232 (15) (2015) 2751–2761. [PubMed: 25772338]

[68]. Scavone JL, Sterling RC, Van Bockstaele EJ, Cannabinoid and opioid interactions: implications for opiate dependence and withdrawal, Neuroscience 248 (2013) 637–654. [PubMed: 23624062]

[69]. Darmani NA, Pandya DK, Involvement of other neurotransmitters in behaviors induced by the cannabinoid CB1 receptor antagonist SR 141716A in naive mice, J. Neural Transm. (Vienna) 107 (8–9) (2000) 931–945. [PubMed: 11041273]

[70]. Schlosburg JE, et al., Endocannabinoid modulation of scratching response in an acute allergenic model: a new prospective neural therapeutic target for pruritus, J. Pharmacol. Exp. Ther 329 (1) (2009) 314–323. [PubMed: 19168707]

[71]. Janoyan JJ, Crim JL, Darmani NA, Reversal of SR 141716A-induced head-twitch and ear-scratch responses in mice by delta 9-THC and other cannabinoids, Pharmacol. Biochem. Behav 71 (1–2) (2002) 155–162. [PubMed: 11812518]

[72]. Lichtman AH, et al., Opioid and cannabinoid modulation of precipitated withdrawal in delta(9)-tetrahydrocannabinol and morphine-dependent mice, J. Pharmacol. Exp. Ther 298 (3) (2001) 1007–1014. [PubMed: 11504797]

[73]. Trexler KR, et al., Novel behavioral assays of spontaneous and precipitated THC withdrawal in mice, Drug Alcohol Depend. 191 (2018) 14–24. [PubMed: 30071445]

[74]. Seltzman HH, et al., Peripherally selective cannabinoid 1 receptor (CB1R) agonists for the treatment of neuropathic pain, J. Med. Chem 59 (16) (2016) 7525–7543. [PubMed: 27482723]

[75]. LoVerme J, et al., Rapid broad-spectrum analgesia through activation of peroxisome proliferator-activated receptor-alpha, J. Pharmacol. Exp. Ther 319 (3) (2006) 1051–1061. [PubMed: 16997973]

[76]. Hamtiaux L, et al., The association of N-palmitoylethanolamine with the FAAH inhibitor URB597 impairs melanoma growth through a supra-additive action, BMC Cancer 12 (2012) 92. [PubMed: 22429826]

[77]. Hamtiaux L, et al., Increasing antiproliferative properties of endocannabinoids in N1E-115 neuroblastoma cells through inhibition of their metabolism, PLOS One 6 (10) (2011) e26823. [PubMed: 22046372]

[78]. Wasilewski A, et al., Fatty acid amide hydrolase (FAAH) inhibitor PF-3845 reduces viability, migration and invasiveness of human colon adenocarcinoma Colo-205 cell line: an in vitro study, Acta Biochim. Pol 64 (3) (2017) 519–525. [PubMed: 28850633]

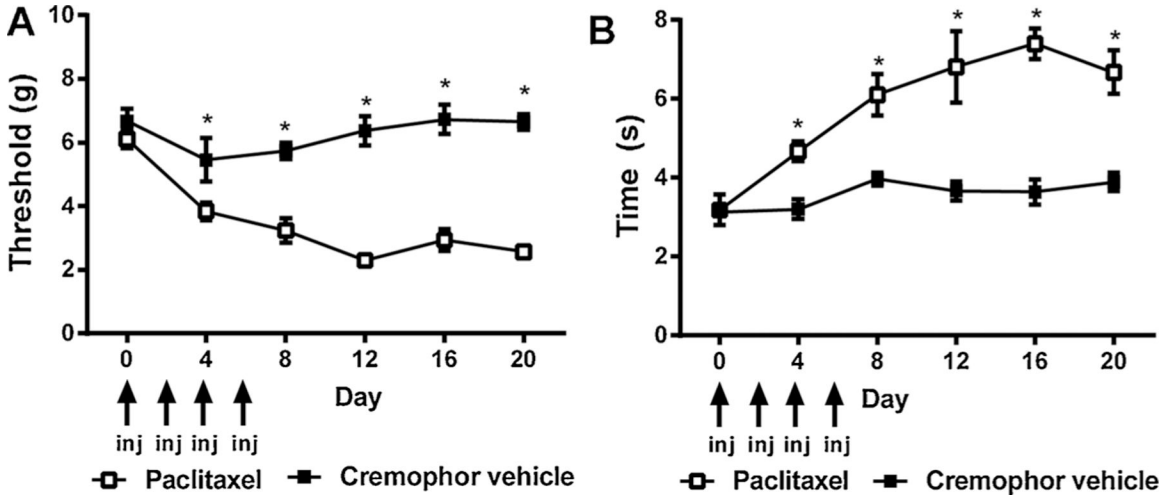

Fig. 1.

Paclitaxel treatment produces hypersensitivities to mechanical and cold stimulation.

Treatment with the chemotherapeutic agent paclitaxel (4 mg/kg i.p. on days 0, 2, 4, and 6) results in hypersensitivities to (A) mechanical and (B) cold stimulation. Data are expressed as mean ± SEM ($n = 5–6$ per group) *$p < 0.05$ vs. cremophor vehicle, two-way repeated measures ANOVA followed by *Bonferroni* post hoc. Arrows denote days when paclitaxel or cremophor vehicle was administered.

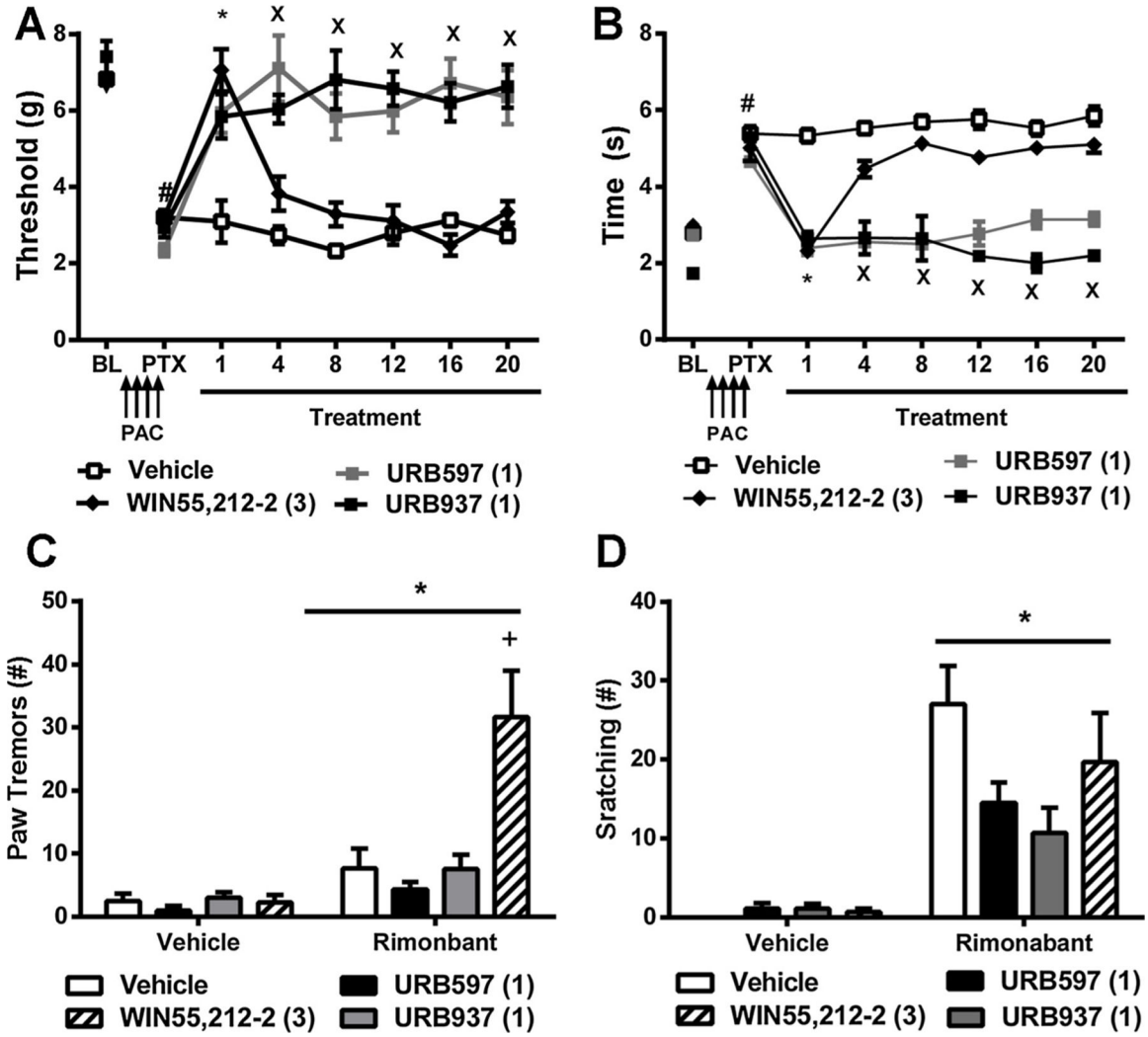

Fig. 2.

Brain permeant and impermeant hibitors of FAAH reduce the maintenance of paclitaxel-induced allodynia. Therapeutic treatment with the brain permeant FAAH inhibitor URB597 (1 mg/kg i.p. × 20 days) and the brain impermeant FAAH inhibitor URB937 (1 mg/kg i.p. × 20 days) reduced paclitaxel-induced (A) mechanical and (B) cold hypersensitivities. By contrast, the pan-cannabinoid agonist WIN55,212–2 (3 mg/kg i.p. × 20 days) initially produced anti-allodynic efficacy but tolerance developed by day 4 of repeated dosing. Rimonabant (10 mg/kg i.p.) challenge increased the number of bouts of (C) paw tremors and (D) scratching behaviors. Rimonabant challenge increased the number of bouts of paw tremors in paclitaxel-treated mice that received WIN55,212–2 but not URB597 or URB937. Data are expressed as mean ± SEM ($n = 5–6$ per group). (A, B) $^{*}p < 0.05$ all groups vs. vehicle, $^{X}p < 0.05$ URB597, URB937 vs. vehicle, Two-way repeated measures ANOVA followed by *Bonferroni* post hoc test. $^{\#}p < 0.05$ vs. pre-paclitaxel baseline, paired two-tailed *t*-test. (C, D) $^{*}p < 0.05$ vs. vehicle challenge, two-way ANOVA, $^{+}p < 0.05$ vs. all groups two-way ANOVA followed by *Bonferroni* post hoc test.

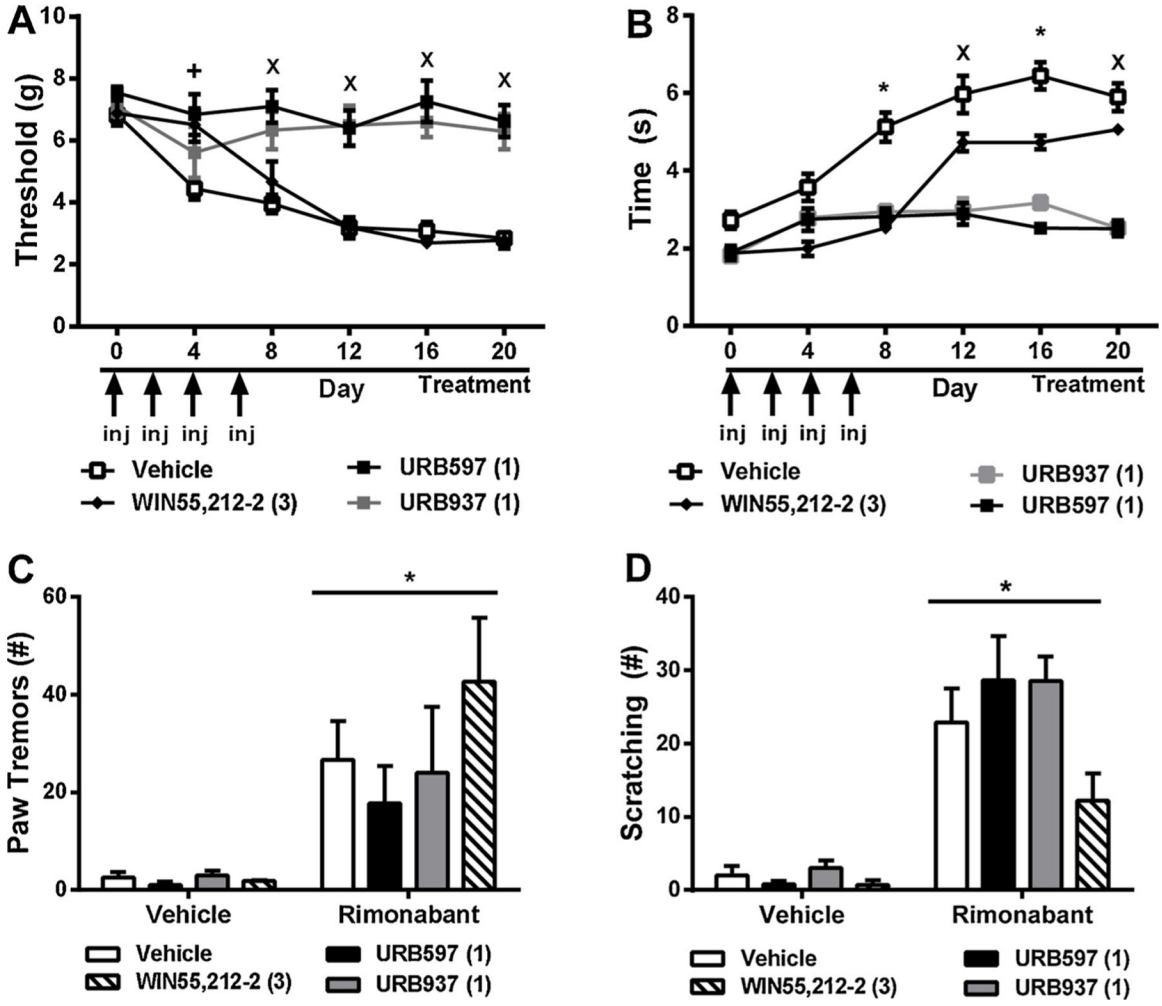

Fig. 3.

Brain permeant and impermeant inhibitors of FAAH prevent the development of paclitaxel-induced allodynia. Prophylactic dosing with the brain permeant FAAH inhibitor URB597 (1 mg/kg i.p. × 20 days) and the brain impermeant FAAH inhibitor URB937 (1 mg/kg i.p. × 20 days) suppresses the development of paclitaxel-induced (A) mechanical and (B) cold hypersensitivities with similar efficacy. By contrast, the orthosteric cannabinoid agonist WIN55,212–2 (3 mg/kg i.p. × 20 days) initially suppressed paclitaxel-induced mechanical and cold hypersensitivity although tolerance developed to the observed antinociceptive effects. Rimonabant (10 mg/kg i.p.) challenge increased the number of bouts of (C) paw tremors and (D) scratching behaviors. Drug treatment did not alter the expression of either behavior. Data are expressed as mean ± SEM ($n = 5–6$ per group) $^{*}p < 0.05$ all groups vs. vehicle, $^{X}p < 0.05$ URB597, URB937 vs. vehicle two-way repeated measures ANOVA followed by *Bonferroni* post hoc. (C, D) $^{*}p < 0.05$ vs. vehicle challenge, two-way repeated measures ANOVA, $^{+}p < 0.05$ vs. all groups two-way ANOVA followed by *Bonferroni* post hoc test.

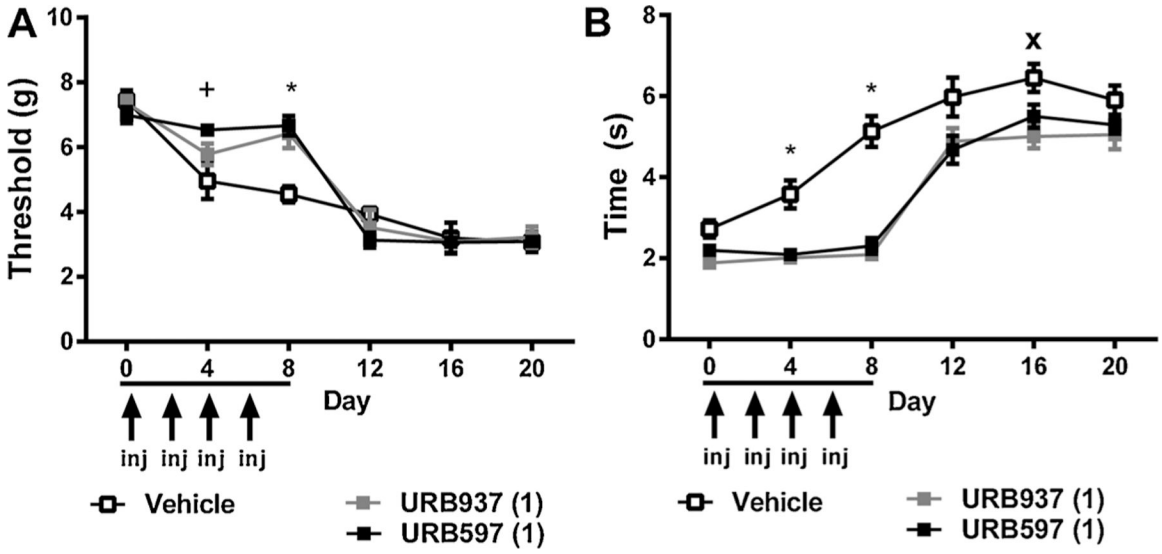

Fig. 4.

Brain permeant and impermeant inhibitors of FAAH delay, but do not prevent, the development of paclitaxel-induced allodynia. The brain permeant FAAH inhibitor URB597 (1 mg/kg i.p. × 8 days) and the brain impermeant FAAH inhibitor URB937 (1 mg/kg i.p. × 8 days), administered over 8 days coincident with initiation of paclitaxel dosing, delayed the onset of paclitaxel-induced (A) mechanical and (B) cold hypersensitivities. Following the cessation of dosing with either URB597 or URB937, paclitaxel-induced allodynia emerges with a magnitude identical to that observed in vehicle-treated animals. Baseline responding, determined on day 0, was assessed prior to dosing with either the aforementioned pharmacological treatments or paclitaxel. Data are expressed as mean ± SEM (n = 5–6 per group). *p < 0.05 all groups vs. vehicle, +p < 0.05 URB597, WIN55,212–2 vs. vehicle, ^{X}p < 0.05 URB597, URB937 vs. vehicle Two-way repeated measures ANOVA followed by *Bonferroni* post hoc test.

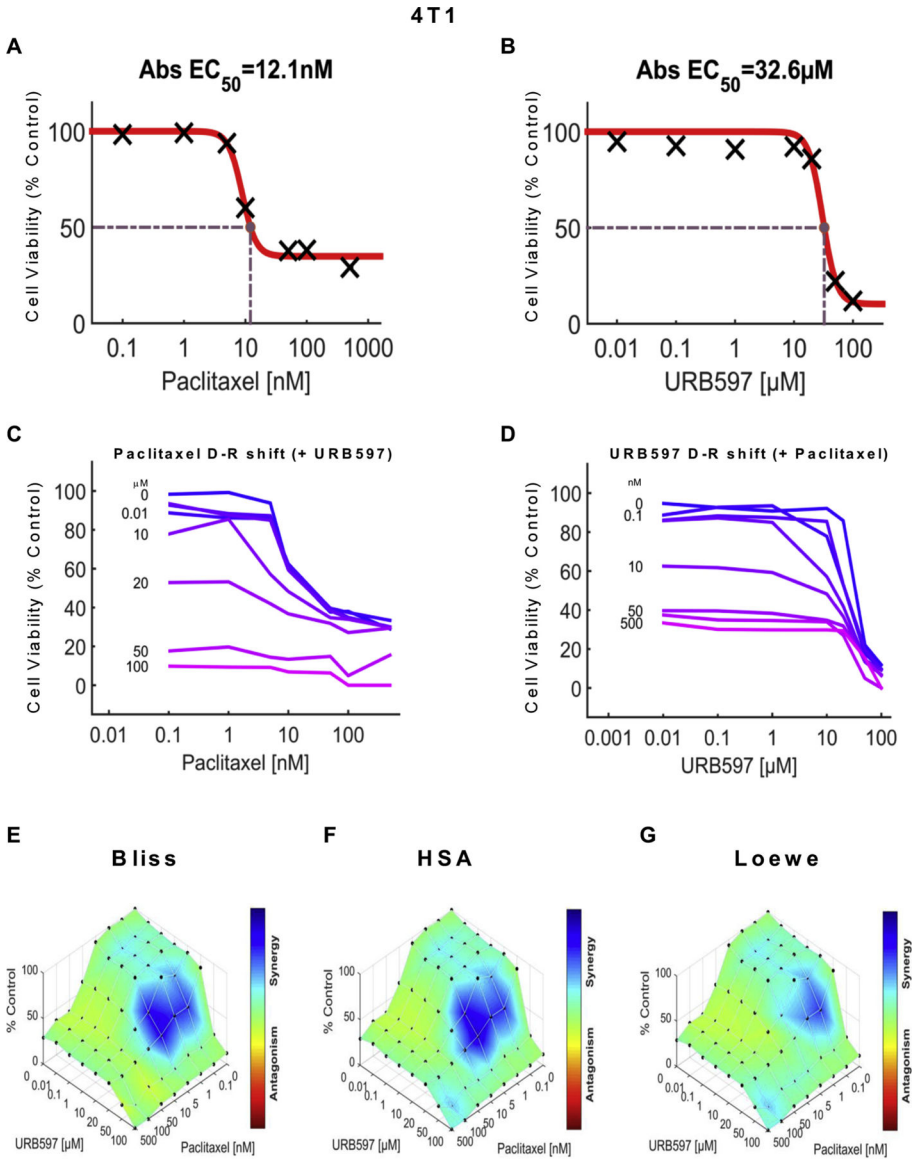

Fig. 5.

URB597 synergizes with paclitaxel in 4T1 cells to reduce breast cancer tumor cell line viability. Dose-response curve showing the effect of (A) paclitaxel and (B) URB597 on tumor cell viability in 4T1 cells. Abs EC_{50}, Absolute EC_{50} = 12.1 nM, reflects efficacy of paclitaxel in reducing 4T1 tumor cell viability by 50% of maximum. Abs EC_{50}, Absolute EC_{50} = 32.6 μM, reflects efficacy of URB597 in reducing 4T1 tumor cell viability by 50% of maximum. (C, D) Single-agent and combination responses determined by an MTT viability assay in 4T1 cells. (C) Paclitaxel dose response shift observed in the presence of increasing concentrations of URB597. (D) URB597 dose response shift observed in the presence of increasing concentrations of paclitaxel. (E–G) The 3-dimensional landscape of the dose matrix is represented on a color scale, where blue reflects evidence of synergy and red reflects evidence of antagonism. The landscape of the dose matrix of combination responses for URB597 and paclitaxel based on the (E) Bliss model, (F) Highest Single

Agent (HSA) model and (G) Loewe model. Each model supports synergy of the combination in reducing 4T1 tumor cell line viability. Cell viability is plotted as % control (n = 3 experiments).

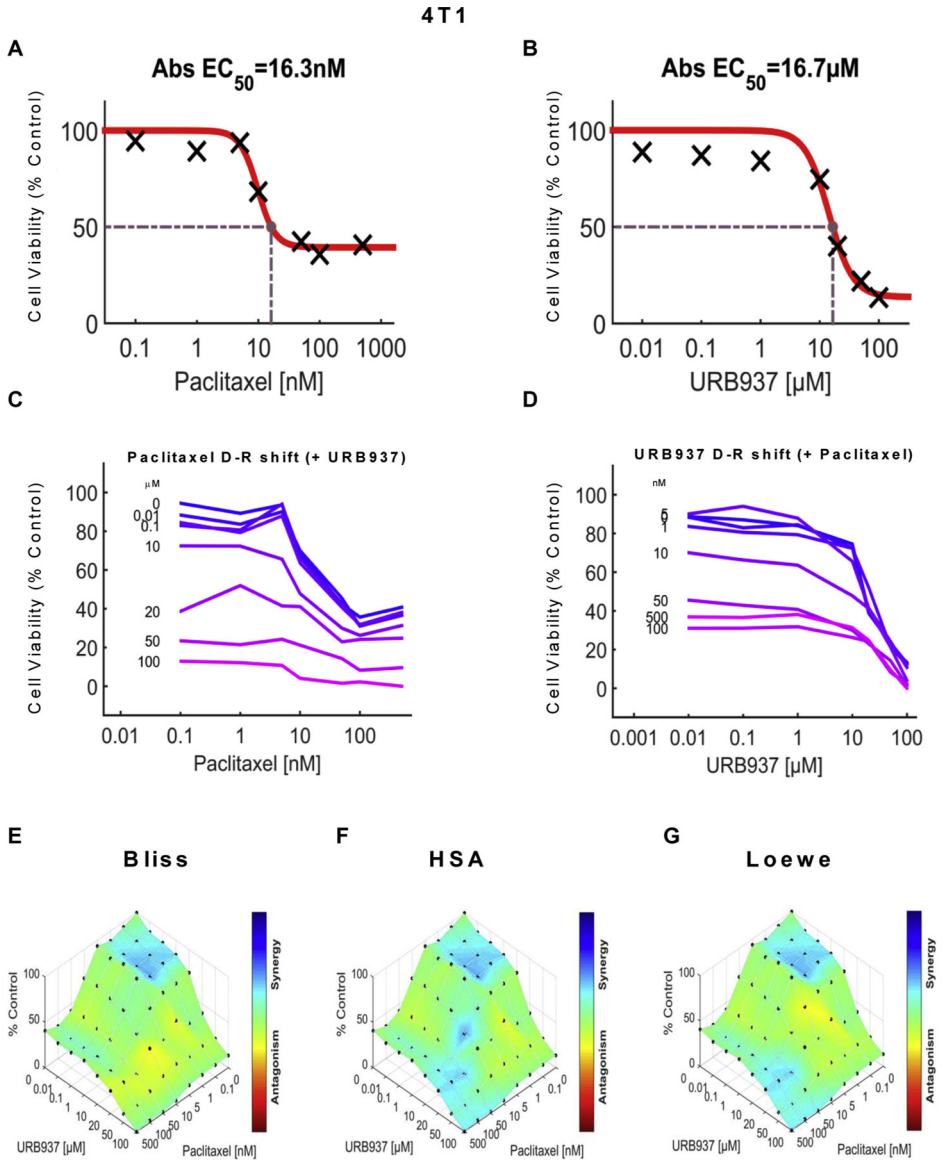

Fig. 6.

URB937 synergizes with paclitaxel in 4T1 cells to reduce breast cancer tumor cell line viability. Dose-response curve for the effect of (A) paclitaxel and (B) URB937 in 4T1 cells. Abs EC_{50}, Absolute EC_{50} = 16.3 nM, reflects efficacy of paclitaxel in reducing 4T1 tumor cell viability by 50% of maximum. Abs EC_{50}, Absolute EC_{50} = 16.7 μM, reflects efficacy of URB937 in reducing 4T1 tumor cell viability by 50% of maximum. (C-D) Single-agent and combination responses determined by an MTT viability assay in 4T1 cells. (C) Paclitaxel dose response shift observed in the presence of increasing concentrations of URB937. (D) URB937 dose response shift observed in the presence of increasing concentrations of paclitaxel. (E–G) The 3-dimensional landscape of the dose matrix is represented on a color scale, where blue reflects evidence of synergy and red reflects evidence of antagonism. The landscape of the dose matrix of combination responses for URB937 and paclitaxel based on the (E) Bliss model, (F) Highest Single Agent (HSA) model and (G) Loewe model. Each

model supports synergy of the combination in reducing 4T1 tumor cell line viability. Cell viability is plotted as % control. (n = 3 experiments).

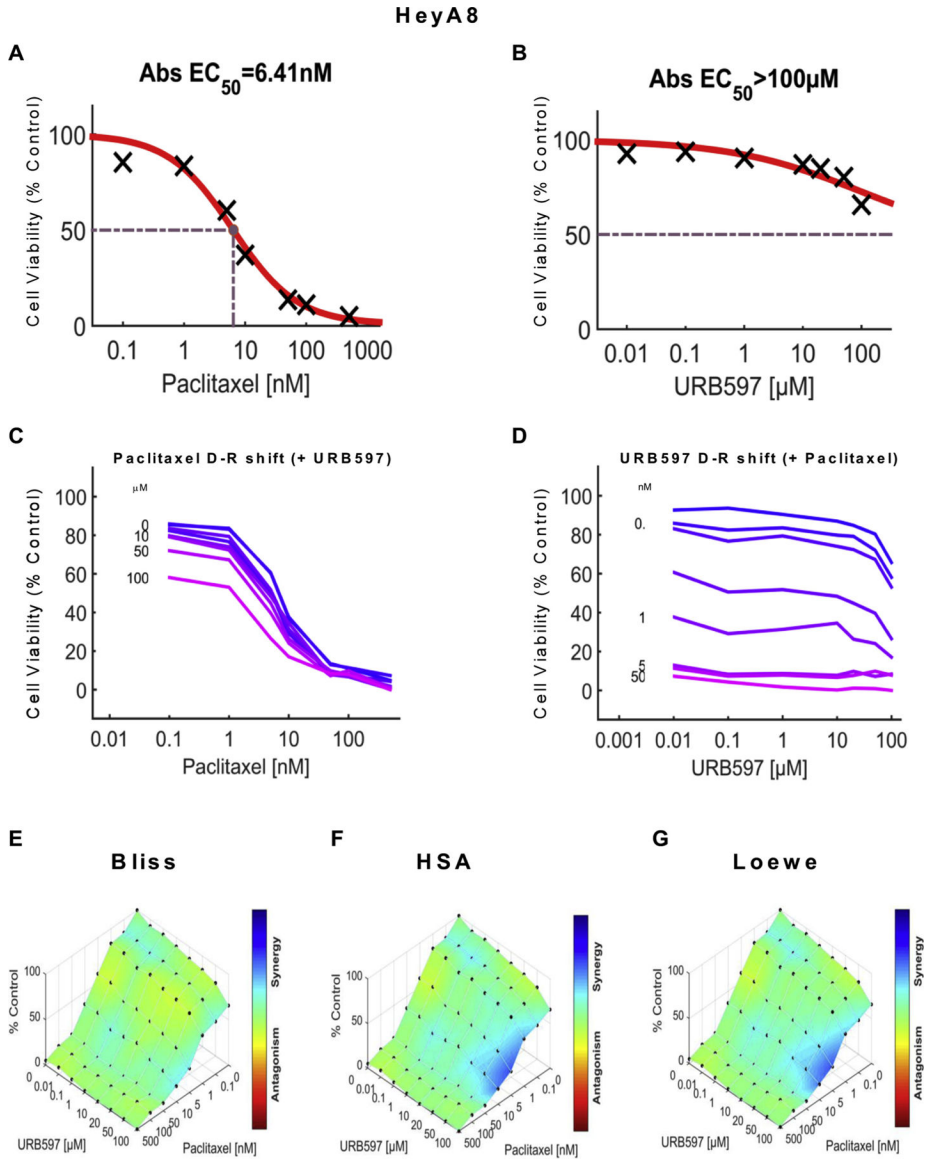

Fig. 7.

URB597 synergizes with paclitaxel to reduce ovarian cancer tumor cell line viability in HeyA8 cells. Dose-response curve for the effect of (A) paclitaxel and (B) URB597 in HeyA8 cells. Abs EC50, Absolute EC_{50} = 6.41 nM, reflects efficacy of paclitaxel in reducing HeyA8 tumor cell viability by 50% of maximum. Abs EC_{50}, Absolute EC_{50} > 100 μM, reflects little or no inhibition of HeyA8 tumor cell viability by URB597. (C, D) Single-agent and combination responses determined by an MTT viability assay in HeyA8 cells. (C) Paclitaxel dose response shift observed in the presence of increasing concentrations of URB597. (D) URB597 dose response shift observed in the presence of increasing concentrations of paclitaxel. (E–G) The 3-dimensional landscape of the dose matrix is represented on a color scale, where blue reflects evidence of synergy and red reflects evidence of antagonism. The landscape of the dose matrix combination responses for URB597 and paclitaxel based on the (E) Bliss model, (F) Highest Single Agent (HSA)

model and (G) Loewe model. Each model supports synergy of the combination in reducing HeyA8 tumor cell line viability. Cell viability is plotted as % control. (n = 3 experiments).

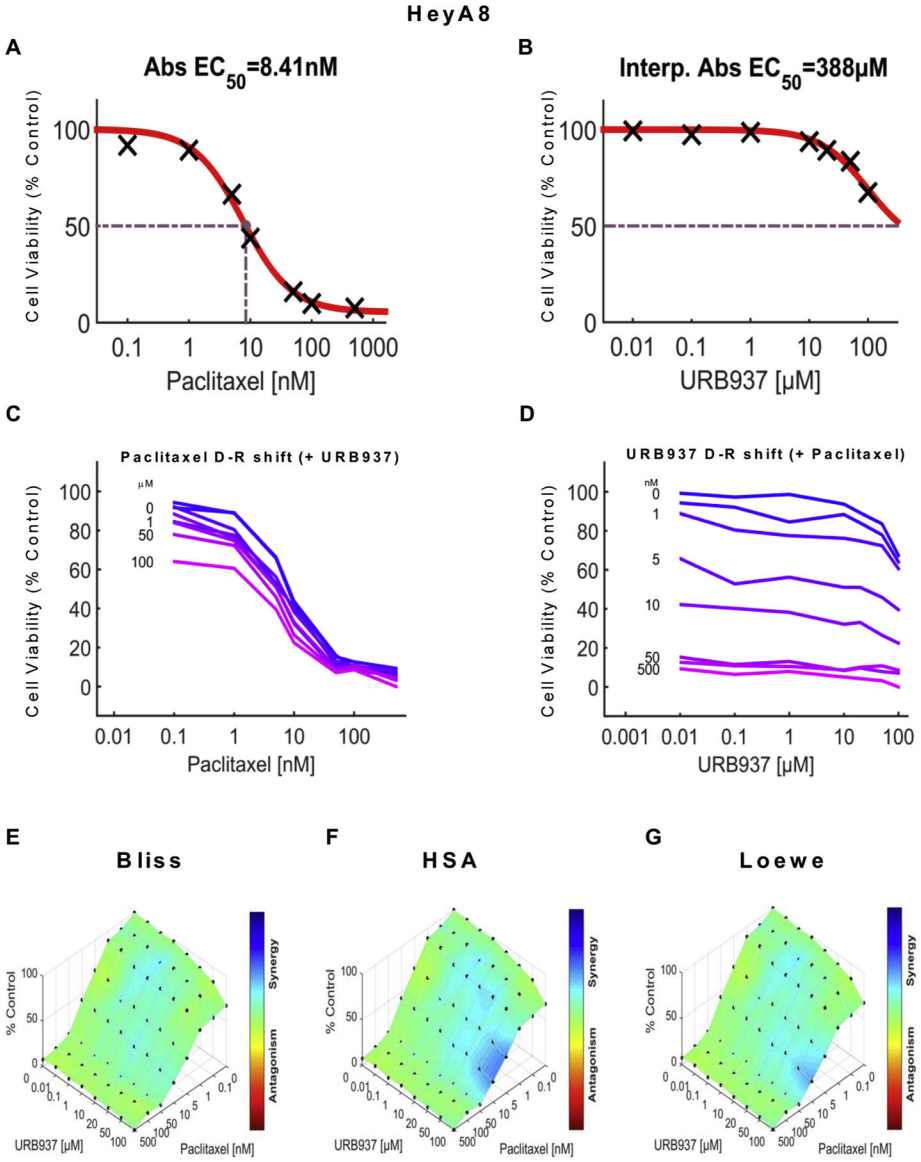

Fig. 8.

URB937 synergizes with paclitaxel to reduce ovarian cancer tumor cell line viability in HeyA8 cells. Dose-response curve for the effect of (A) paclitaxel and (B) URB937 in HeyA8 cells. Abs EC_{50}, Absolute EC_{50} = 8.41 nM, reflects efficacy of paclitaxel in reducing HeyA8 tumor cell viability by 50% of maximum. Interp. Abs EC_{50}, Interpolated Absolute EC_{50} = 388 μM, reflects little or no inhibition of HeyA8 tumor cell viability by URB937. (C, D) Single-agent and combination responses determined by an MTT viability assay in HeyA8 cells. (C) Paclitaxel dose response shift observed in the presence of increasing concentrations of URB937. (D) URB937 dose response shift observed in the presence of increasing concentrations of paclitaxel. (E–G) The 3-dimensional landscape of the dose matrix is represented on a color scale, where blue reflects evidence of synergy and red reflects evidence of antagonism. The landscape of the dose matrix combination responses for URB937 and paclitaxel based on the (E) Bliss model, (F) Highest Single Agent (HSA)

model and (G) Loewe model. Each model supports synergy of the combination in reducing HeyA8 tumor cell line viability. Cell viability is plotted as % control ($n = 3$ experiments).

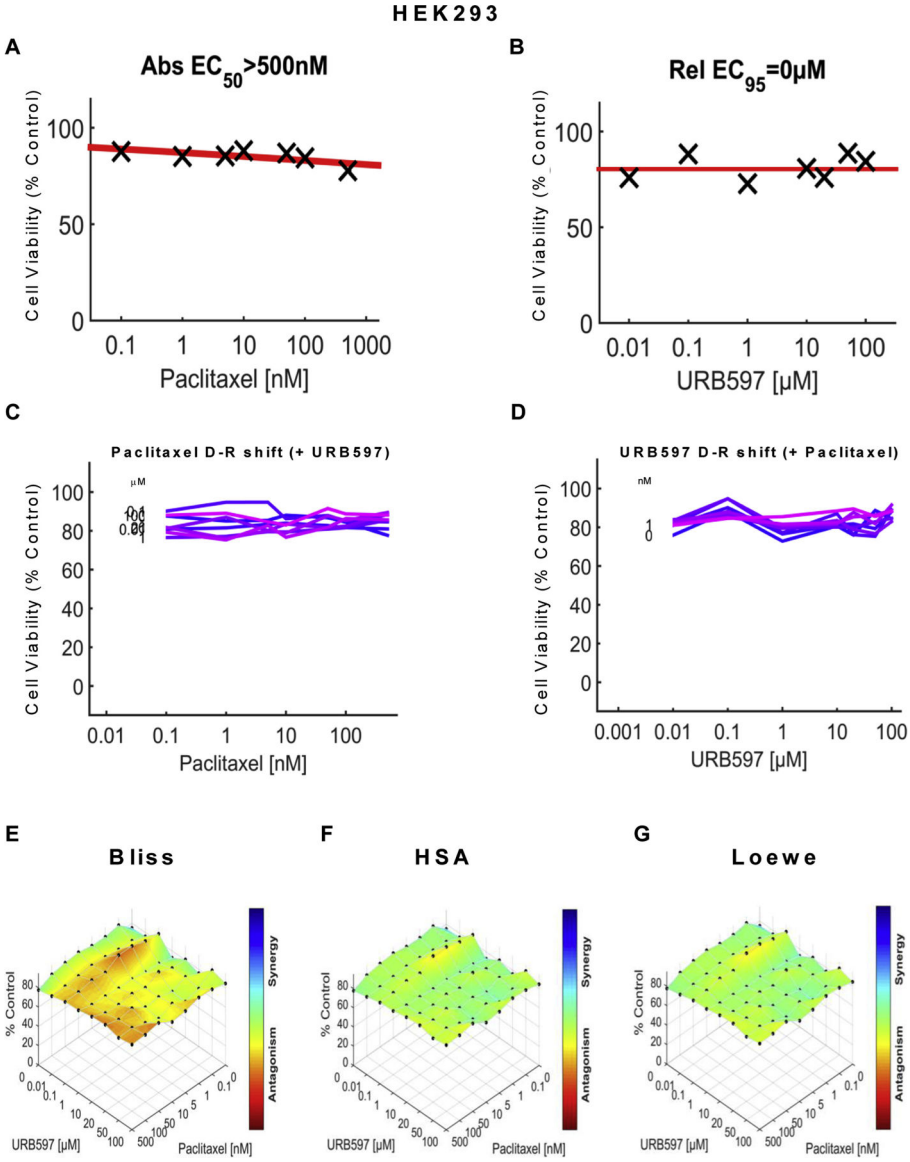

Fig. 9.

URB597 does not inhibit viability of non-tumor HEK293 cells in the presence or absence of paclitaxel. Dose-response curve for the effect of (A) paclitaxel and (B) URB597 on viability of HEK293 cells. Abs EC_{50}, Absolute EC_{50} > 500 nM, reflects no inhibition of HEK293 cell viability by URB597 at the highest concentration tested; Rel EC_{95}, relative EC_{95} =0 μM, reflects absence of inhibition of HEK293 cell viability by URB597 at the highest concentration tested. (C, D) Single-agent and combination responses determined by an MTT viability assay in HEK293 cells. (C) Paclitaxel dose response shift observed in the presence of increasing concentrations of URB597. (D) URB597 dose response shift observed in the presence of increasing concentrations of paclitaxel. (E–G) The 3-dimensional landscape of the dose matrix is represented on a color scale, where blue reflects evidence of synergy and red reflects evidence of antagonism. The landscape of the dose matrix combination responses for URB597 and paclitaxel based on the (E) Bliss model, (F) Highest Single

Agent (HSA) model and (G) Loewe model. Cell viability is plotted as % control ($n = 3$ experiments).

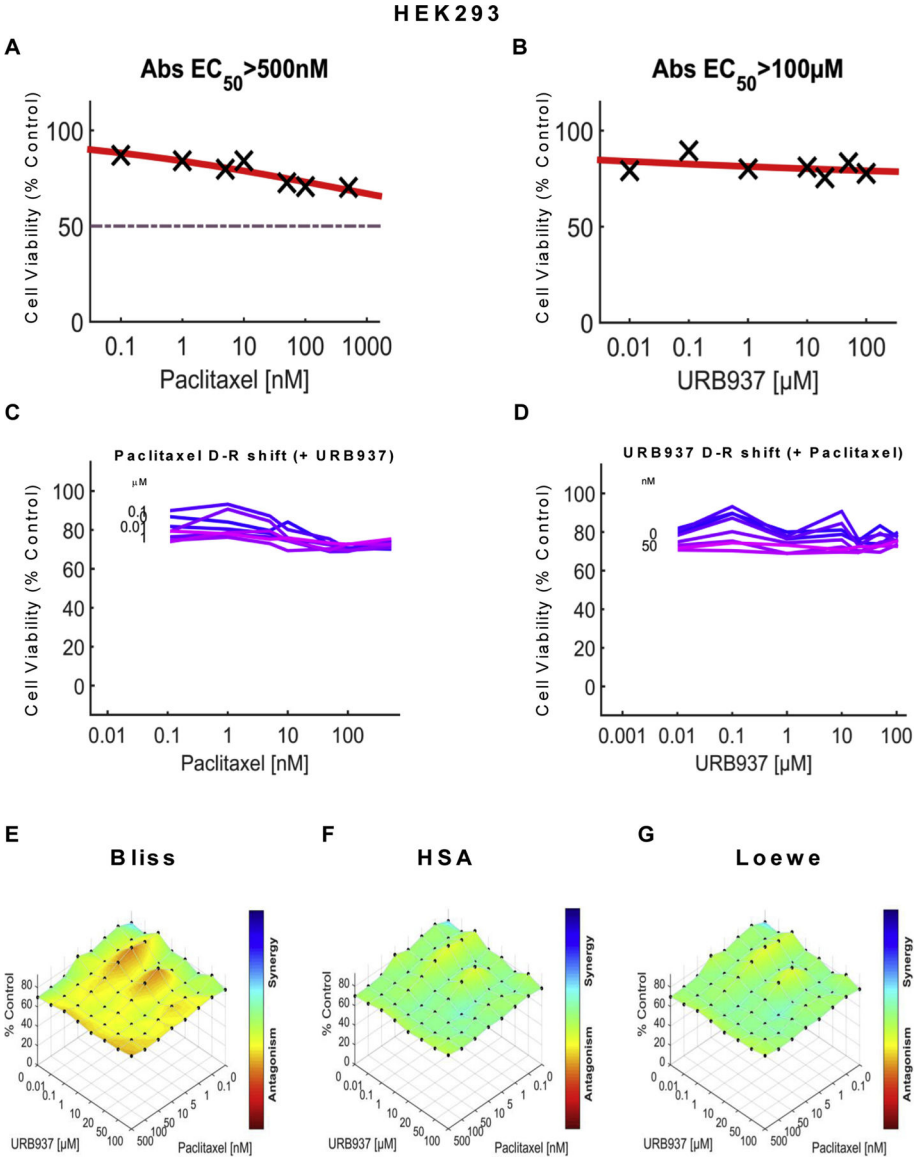

Fig. 10.

URB937 has no effect on cell line viability in HEK293 cells in the presence or absence of paclitaxel. Dose-response curve for the effect of (A) paclitaxel and (B) URB937 in HEK293 cells. Abs EC_{50}, Absolute EC_{50} > 500 nM, reflects no inhibition of HEK293 cell viability by paclitaxel at the highest concentration tested; Abs EC_{50}, Absolute EC_{50} > 100 μM, reflects little or no inhibition of HEK293 cell viability by URB937 at the highest concentration tested. (C, D) Single-agent and combination responses determined by an MTT viability assay in HEK293 cells. (C) Paclitaxel dose response shift observed in the presence of increasing concentrations of URB937. (D) URB937 dose response shift observed in the presence of increasing concentrations of paclitaxel. (E–G) The 3-dimensional landscape of the dose matrix is represented on a color scale, where blue reflects evidence of synergy and red reflects evidence of antagonism. The landscape of the dose matrix combination responses for URB937 and paclitaxel based on the (E) Bliss model, (F) Highest Single

Agent (HSA) model and (G) Loewe model. Cell viability is plotted as % control ($n = 3$ experiments).

Table 1

FAAH inhibitors synergize with paclitaxel to increase 4T1 and HeyA8 tumor cell line cytotoxicity but lack cytotoxic effects in non-tumor HEK293 cell lines.

		Combination with Paclitaxel		
Cell line	**FAAH Inhibitor**	**Model**	**Synergy Score**	**Most synergistic area score**
4T1	URB597	Bliss	5.31	21.59
		HSA	7.34	20.82
		Loewe	N/A *	N/A *
	URB937	Bliss	0.73	3.99
		HSA	4.55	13.99
		Loewe	0.10	13.84
HeyA8	URB597	Bliss	5.19	10.87
		HSA	7.15	18.41
		Loewe	26.81	46.89
	URB937	Bliss	5.05	11.40
		HSA	6.63	16.71
		Loewe	32.33	53.36
HEK293	URB597	Bliss	−4.90	2.04
		HSA	−4.43	1.70
		Loewe	−3.67	0.62
	URB937	Bliss	−2.31	1.22
		HSA	0.46	3.52
		Loewe	N/A *	N/A *

Data (derived from duplicate determinations from $n = 3$ experiments performed on different days) was evaluated using Synergyfinder to generate both the synergy score and the most synergistic area score. Positive scores reflect evidence of synergy whereas negative scores reflect antagonism.

* Loewe model is not able to calculate the synergy score with this combination data set.